Check for updates

Original Article

Biofpr Biofuels Bioproducts & Biorefining

Exploring quinolinone–chalcones: Synthesis, antioxidant potential and industrial applications in biofuels

Vitor S. Duarte, Renata Layse G. de Paula, Leonardo R. Almeida, Grupo de Química Teórica e Estrutural de Anápolis, Universidade Estadual de Goiás, Anápolis, Brazil
Giulio D. C. D'Oliveira, Caridad N. Pérez, Instituto de Química, Universidade Federal de Goiás, Goiânia, Brazil
Jean M. F. Custódio, Valter H. Carvalho-Silva, Grupo de Química Teórica e Estrutural de Anápolis, Universidade Estadual de Goiás, Anápolis, Brazil
Andrea Lombardi, Dipartimento di Chimica, Biologia e Biotecnologie, Università di Perugia, Perugia, Italy
Hamilton B. Napolitano, Grupo de Química Teórica e Estrutural de Anápolis, Universidade Estadual de Goiás, Anápolis, Brazil

Received November 4 2024; Revised March 18 2025; Accepted March 24 2025;
View online at Wiley Online Library (wileyonlinelibrary.com);
DOI: 10.1002/bbb.2774; *Biofuels, Bioprod. Bioref.* (2025)

Abstract: Biofuels undergo oxidative degradation, which reduces their storage stability and efficiency, hindering their large-scale adoption and integration into the global energy matrix. To address this issue, we synthesized and characterized four novel quinolinone–chalcone derivatives (substituted with Br, Cl, OCH_3 and OCH_2CH_3) as potential antioxidant additives. Structural analysis, density functional theory calculations and machine learning-based hydroxyl radical scavenging rate evaluation were performed to assess the influence of the substituents on stability and antioxidant capacity. Single-crystal X-ray diffraction revealed C–H···O and C–H···π interactions contributing to supramolecular stability, while electronic property analysis indicated enhanced kinetic stability and regions near the sulfonamide group prone to nucleophilic attack. Machine learning predictions showed that the bromine derivative exhibited a hydroxyl radical scavenging rate of $7.97 \times 10^9\ M^{-1}\ s^{-1}$, comparable with the commercial antioxidant butylated hydroxytoluene ($4.34 \times 10^9\ M^{-1}\ s^{-1}$). These findings highlight the potential of quinolinone–chalcone derivatives as efficient antioxidant additives, improving the oxidative stability and sustainability of biofuels. © 2025 The Author(s). *Biofuels, Bioproducts and Biorefining* published by Society of Industrial Chemistry and John Wiley & Sons Ltd.

Supporting information may be found in the online version of this article.

Key words: biofuels; oxidative stability; quinolinone–chalcones; machine learning

Correspondence to: Vitor S. Duarte and Hamilton B. Napolitano, Grupo de Química Teórica e Estrutural de Anápolis, Universidade Estadual de Goiás, Anápolis, GO, Brazil. E-mail: vitorvsd132@gmail.com and hbnapolitano@gmail.com

SCI where science meets business

© 2025 The Author(s). *Biofuels, Bioproducts and Biorefining* published by Society of Industrial Chemistry and John Wiley & Sons Ltd. This is an open access article under the terms of the Creative Commons Attribution License, which permits use, distribution and reproduction in any medium, provided the original work is properly cited.

19321031, 0, Downloaded from https://scijournals.onlinelibrary.wiley.com/doi/10.1002/bbb.2774 by Capes, Wiley Online Library on [28/08/2025]. See the Terms and Conditions (https://onlinelibrary.wiley.com/terms-and-conditions) on Wiley Online Library for rules of use; OA articles are governed by the applicable Creative Commons License

Introduction

The planned synthesis of bioactive compounds is the initial step in product development, and we have found several promising classes of compounds described in the literature with potential biological activities. Quinolinones represent a class of bicyclic nitrogen-containing heterocycles that have attracted increasing interest in scientific research owing to their diverse biological and chemical activities.[1,2] These compounds, structurally derived from quinoline, feature a benzene ring fused to a pyridine ring and are known for their chemical stability and multifunctional properties.[3–5] In recent years, quinolinones and their derivatives (such as quinolinone–chalcones) have been explored for their potential industrial applications, including potential antioxidant activity,[6–15] as well as antimicrobial activity.[16–25] These described properties are desirable in new drugs, new materials and new additives. For biofuels, such properties could prevent fuel oxidation and combat the proliferation of microorganisms that degrade them.[26,27]

With the increasing demand for sustainable energy sources and the need to reduce dependence on fossil fuels, biofuels have emerged as a promising alternative.[28–31] However, one of the main challenges in using biofuels is their susceptibility to oxidation, which can compromise fuel efficiency and lead to the formation of undesirable subproducts, such as carboxylic acids and insoluble polymers, resulting in corrosion and clogging of fuel injection systems.[26,27,32–34] In this context, quinolinones and their derivatives can be studied as potential additives owing to their antioxidant and antimicrobial properties. The antioxidant activity of quinolinones can be associated with their ability to donate electrons or hydrogen atoms, neutralizing free radicals and interrupting oxidation chain reactions.[35–39]

Recent studies indicate that chalcones (compounds that can be hybridized with quinolinones) can be used as additives in biofuels, significantly improving their oxidative stability, prolonging their shelf life, and enhancing fuel efficiency.[40–43] A study conducted by Carapina *et al.* (2018)[44] demonstrated the influence of chalcones on the antioxidation of biodiesel, resulting in a significant improvement in the fuel's oxidative stability. Additionally, Moreira *et al.* (2022)[45] showed the antioxidant activity of a tri-methoxy chalcone added to a biodiesel blend, with stability results comparable with those for commercial additives such as BHT (butylated hydroxytoluene). Based on these aspects, hybrid structures like quinolinone–chalcones are promising, but there is still much to explore. New studies are needed to fully understand the antioxidant mechanisms of action of these compounds. Additionally, evaluating the environmental and economic impacts associated with the production and use of these substances is essential to determine their commercial viability. Machine learning (ML) has become important for predictive analysis in molecular chemistry. XGBoost (Extreme Gradient Boosting), known for its efficiency in classification and regression tasks, is widely used to model molecular properties, optimize reactions and predict antioxidant activity.[46,47] In this study, we employ machine learning techniques with XGBoost through the *Py*SIRC platform[48] to predict reaction rate constants and evaluate the physicochemical properties of novel quinolinone chalcones. We synthesized four quinolinone chalcone derivatives (**QC01** to **QC04**) to investigate the influence of different substituents (Br, Cl, OCH_3 and OCH_2CH_3) on their supramolecular arrangement, reactivity and potential applications as additives in biodiesel blends.

Experimental and computational procedures

Synthesis of the quinolinone–chalcones

Compounds **QC01** [2-(4-ethoxyphenyl)-2,3-dihydro-1-(phenylsulfonyl)quinolin-4(1H)-one], **QC02** [2-(4-methoxyphenyl)-2,3-dihydro-1-(phenylsulfonyl) quinolin-4(1H)-one], (**QC03**) 2-(4-chlorophenyl)-2,3-dihydro-1-(phenylsulfonyl)quinolin-4(1H)-one and (**QC04**) 2-(4-bromophenyl)-2,3-dihydro-1-(phenylsulfonyl)quinolin-4(1H)-one were obtained from the synthesis of four chalcones (**CH01** to **CH04**). 2′*N*-Phenylsulfonylacetophenone was synthesized in the first step (intermediate **I01**). The reaction of benzenesulfonyl chloride with 2-aminoacetophenone in dichloromethane (Scheme 1) was carried out following previously described conditions.[49–52] Four 2′*N*-sulfonamide chalcones (**CH01** to **CH04**) were synthesized *via* Claisen–Schmidt condensation between **I01** and a benzaldehyde, using basic catalysis in an ethanolic medium (Scheme 2).

Four quinolinones were prepared (Scheme 3). The cyclized compounds **QC01**, **QC02**, **QC03** and **QC04** were obtained, starting respectively from **CH01**, **CH02**, **CH03** and **CH04**, in high yields and purified by filtration, based on the procedure previously decribed.[51,53]

Procedure for preparing sulfonamide chalcones CH01 to CH04

56.8 mmol (3.187 g) of potassium hydroxide was weighed and dissolved in 3.0 mL of water. Ethanol (400.0 mL) was added to this solution and homogenized. An amount of 20 mmol (5.506 g) of **I01** was added and dissolved. Then the aldehyde was added (40 mmol for the synthesis of the compounds

© 2025 The Author(s). *Biofuels, Bioproducts and Biorefining* published by Society of Industrial Chemistry and John Wiley & Sons Ltd.

CH01, **CH02** and **CH03**, and 21 mmol for the synthesis of the compound **CH04** – 6.007 g of 4-ethoxybenzaldehyde, 5.446 g of 4-methoxybenzaldehyde, 5.623 g of 4-chlorobenzaldehyde and 3.885 g of 4-bromobenzaldehyde, respectively), magnetic stirring started and the reaction timed from that point. The temperature of the system was ambient (near to 25 °C). The reaction progress was tracked using thin-layer chromatography in normal phase, with a hexane and ethyl acetate solution in an 85:15 ratio as the mobile phase. The reactions were quenched by the gradual addition of 37% (w/w) hydrochloric acid in an amount equimolar to potassium hydroxide, while the system remained under stirring. The time elapsed in each reaction was as follows (h:min): **CH01**, 25:30; **CH02**, 2:15; **CH03**, 2:00; and **CH04**, 2:00. The system, after neutralization, was poured into 800 mL of water. It was then extracted with 200 mL of dichloromethane. The organic phase was passed through filter paper containing anhydrous sodium sulfate and left to evaporate slowly. Before fully drying, the crystals were collected and rinsed with ethanol. After drying, they were weighed for yield determination. The yield of each reaction was as follows: **CH01**, 6.20 g (76.1%); **CH02**, 7.36 g (93.5%); **CH03**, 5.64 (70.9%) and **CH04**, 4.61 g (52.0%). For the ^{1}H NMR, ^{13}C NMR, IR and HRMS for **CH1** to **CH4**, see the supplementary information.

General procedure for preparing quinolinones QC01 to QC04

Chalcones **CH01** to **CH04** (200 mg) were weighed, finely ground in a pestle and mortar and transferred to an aqueous solution containing potassium hydroxide (449 mg in 100 mL) and diethylamine (124 µL in 100 mL). The system was kept under agitation for 41 h 30 min, at which point it was no longer possible to verify the presence of chalcone on the thin-layer chromatography plates (normal stationary phase and solution of hexane and ethyl acetate in the proportion of 85:15 as mobile phase); there was just one fluorescent spot under UV light of 366 nm. The precipitate was filtered and washed with water. It was then dissolved in 20 mL of dichloromethane, and the resulting solution was extracted with 20 mL of water. The organic phase was passed through

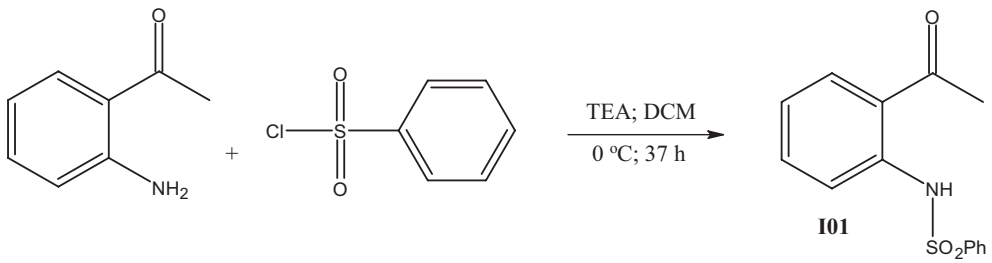

Scheme 1. Representation of conditions for the synthesis of 2'*N*-phenylsulfonylacetophenone (**I01**).

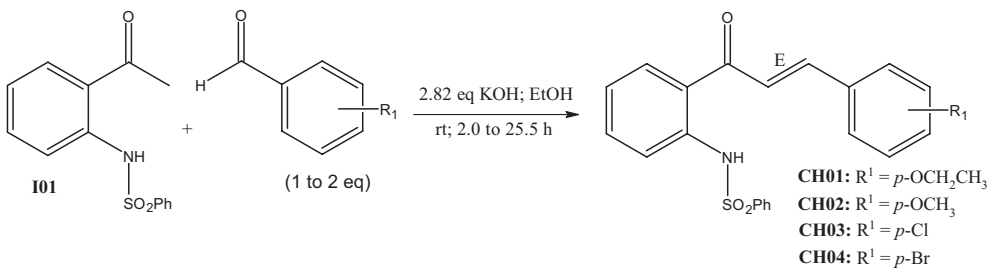

Scheme 2. Representation of Claisen-Schmidt condensation for the synthesis of the chalcones **CH01** to **CH04**.

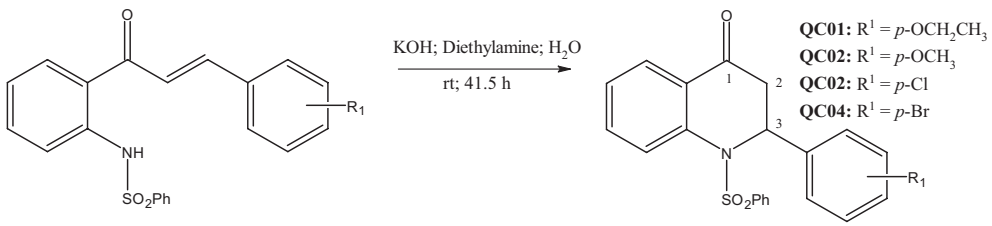

Scheme 3. Synthesis of quinolinones **QC01** to **QC04**.

© 2025 The Author(s). *Biofuels, Bioproducts and Biorefining* published by Society of Industrial Chemistry and John Wiley & Sons Ltd.

19321031, 0, Downloaded from https://scijournals.onlinelibrary.wiley.com/doi/10.1002/bbb.2774 by Capes, Wiley Online Library on [28/08/2025]. See the Terms and Conditions (https://onlinelibrary.wiley.com/terms-and-conditions) on Wiley Online Library for rules of use; OA articles are governed by the applicable Creative Commons License

filter paper containing anhydrous sodium sulfate and left to dry slowly. The mass of products obtained was: **QC01**, 166 mg (82.7%); **QC02**, 196 mg (98.0%): **QC03**, 171 mg (85.5%); **QC04**, 157 mg (78.5%). For the ^{1}H NMR, ^{13}C NMR, and HRMS for **QC01** to **QC04**, see the supplementary information.

Although the chemical process initially originates on a small scale in the laboratory, this yield can be scaled up to a large scale, which is necessary for the chemical industry.[54] Furthermore, the Global Health Innovative Technology determines some criteria for promising molecular successes, such as synthesis in five or fewer steps, acceptable yield and solubility and purity >90%.[55] The quinolinone–chalcones synthesized in the work meet these criteria and present a relatively simple synthesis, and this class of compounds has acceptable solubility in polar and nonpolar solvents.[56]

Solid-state analysis

The crystallographic analysis of the four quinolinone–chalcone compounds was conducted using X-ray diffraction data collected with a Bruker APEX-II CCD diffractometer, employing MoKα radiation ($\lambda = 0.71073$ Å) at 120 K. The structures were solved and refined using SHELX software,[57] implemented on the OLEX2 platform.[58] The crystallographic data for these structures have been deposited in the Cambridge Crystallographic Data Centre[59] under the following deposition numbers: 2393625 (**QC01**), 2 393 627 (**QC02**), 2 393 628 (**QC03**) and 2 393 629 (**QC04**). The representations of molecular interactions for these structures were generated using the Mercury software,[60] based on the geometric parameters experimentally obtained from X-ray diffraction. Additionally, CrystalExplorer software was employed to quantify the molecular interactions in the quinolinone–chalcones, based on electron density through Hirshfeld surfaces.[61] These Hirshfeld surfaces are derived from the normalized contact distances, including the distance from the surface to the nearest atom within the same molecule (*de*) and the distance from the surface to the nearest atom in a neighboring molecule (*di*).[62,63] The 2D fingerprint plots are graphical representations of the *de versus di* distribution.[64]

Theoretical analysis and machine-learning procedures

The theoretical analysis for the quinolinone–chalcones was conducted using density functional theory (DFT).[65] These calculations were performed for both molecular conformations (solid state and gas phase), based on the geometric parameters obtained from X-ray diffraction, utilizing Gaussian09 software[66] at the M06-2X/6–311++G(d, p)[67–69] theory level. From the wave function generated in these calculations, the frontier molecular orbitals were computed, as well as the HOMO (highest occupied molecular orbital) and the LUMO (lowest unoccupied molecular orbital).[70,71] To further investigate the reactive sites of these quinolinone–chalcones, the molecular electrostatic potential (MEP) map was also calculated.[72]

The oxidation reactions by free radicals were simulated using *py*SiRC,[48] a machine-learning platform, selecting the hydroxyl radical (•OH) as a model for oxidative degradation. Predictions of the reaction rate constant (k_{OH}) in B20 blends were generated using the Morgan and MACCS fingerprints combined with the trained model under XGBoost algorithm. In the *py*SiRC[48] platform, input files can be provided in *.txt* format, containing the SMILES identifiers of the molecules (SMILES for **QC01** to **QC04** are shown in the supplementary information – Table S1). The authors applied XGBoost – a method based on a gradient-boosting decision tree,[46] one algorithm among others that they used to predict the kinetic constant of organic pollutants in the aqueous phase. This algorithm has a database built for the reaction rate constants of an oxidative process mediated by the •OH radical, formed by a group of 1374 parameters (k_{OH}) for organic compounds. The referred kinetic parameters are catalogued under standard conditions, 25 °C and 1 mol·L^{-1} in the aqueous phase. This algorithm was developed under the same Gradient Boosting framework, aiming to be highly efficient, flexible and portable. XGBoost provides a parallel tree reinforcement that solves many data science problems quickly and accurately and has therefore been widely used in recent literature.[73–76] The performance indices – correlation coefficient (R^2), Pearson correlation coefficient of prediction (r^2), root-mean-square deviation (RMSE), and external validation (Q^2_{ext}) – were calculated using the formulas:

$$R^2 = 1 - \frac{\sum_{i=1}^{n}\left(y_{exp} - y_{pred}\right)^2}{\sum_{i=1}^{n}\left(y_{exp} - \bar{y}_{exp}\right)^2} \quad (1)$$

$$r^2 = \frac{\sum_{i=1}^{n}\left(y_{exp} - \bar{y}_{exp}\right)\cdot\left(y_{pred} - \bar{y}_{pred}\right)}{\sqrt{\sum_{i=1}^{n}\left(y_{exp} - \bar{y}_{exp}\right)^2}\sqrt{\sum_{i=1}^{n}\left(y_{pred} - \bar{y}_{pred}\right)^2}} \quad (2)$$

$$\mathrm{RMSE} = \sqrt{\frac{\sum_{i=1}^{n}\left(y_{exp} - y_{pred}\right)^2}{n}} \quad (3)$$

© 2025 The Author(s). *Biofuels, Bioproducts and Biorefining* published by Society of Industrial Chemistry and John Wiley & Sons Ltd.

19321031, 0, Downloaded from https://scijournals.onlinelibrary.wiley.com/doi/10.1002/bbb.2774 by Capes, Wiley Online Library on [28/08/2025]. See the Terms and Conditions (https://onlinelibrary.wiley.com/terms-and-conditions) on Wiley Online Library for rules of use; OA articles are governed by the applicable Creative Commons License

$$Q^2_{ext} = 1 - \frac{\sum_{i=1}^{n} \left(y_{exp} - y_{pred}\right)^2}{\sum_{i=1}^{n} \left(y_{exp} - \overline{y}^{tr}_{exp}\right)^2} \quad (4)$$

where y_{exp}, y_{pred}, $\overline{y}_{exp}$ and $\overline{y}_{pred}$ are the experimental, predicted and average of the experimental and predicted values of the dependent variable (over the validation set), respectively, and $\overline{y}^{tr}_{exp}$ is the average value of the dependent variable for the training set – the sums cover all the compounds in the validation set.[48] The authors of *py*SiRC have reported this model by yielding a high goodness-of-fit for training ($R^2 > 0.937$) and good predictive accuracy for the test set ($R^2_{ext} = Q^2_{ext}$ in the 0.707–0.823 range).[48] The hyperparameters of the machine learning model (XGBoost) used in *py*SiRC were: base score (0.5); booster (gbtree); gamma (0); learning_rate (0.3); max delta step (0); max depth (6); Number of gradient boosted trees (150); alpha (0); lambda (1).

The applicability domain (AD%) indicates the similarity between query compounds and the database, supporting the model's reliability.[48] The *Tanimoto* index[77] was used to evaluate the similarity between the compounds in the work, according to the following equation:

$$T_c(A, B) = \frac{c}{a + b - c} \quad (5)$$

where a and b are the number of structural features for compound A and B compared, or bits set to 1, in each molecule, and c is the number in common.

The k_{OH} parameters were calculated for major diesel (1-decene) and biodiesel compounds (e.g. methyl 9-octadecenoate, BD M9OD 19.98%; methyl palmitate, BD MPAL 12.87%; and methyl 8,11-octadecenoate, BD M8OD 10.22%)[78] and tested against other antioxidant candidates, including compounds (**QC01**, **QC02**, **QC03** and **QC04**), previously tested additives and commercial additives (BHT, tert-butyl hydroquinone, TBHQ; butylated hydroxyanisole, BHA; propyl gallate, PG; pyrogallol, PY; and gallic acid, GA).[79]

Results and discussion

Solid state description

Evidence of the successful synthesis of compounds **QC01** to **QC04** was the nonobservance in ^{1}H NMR spectra of the signal from sulfonamide hydrogens in the δ 11.3 region. Further evidence was provided by two diastereotopic α-carbonyl hydrogens (H2a and H2b, Scheme 3), with a geminal coupling of 17.9 Hz. These hydrogens are coupled with vicinal hydrogen (H3) with coupling constants near to 6.0 and 1.7 Hz, for *cis* and *trans* respectively (Figs S1–S12). All of these structures were confirmed through single-crystal X-ray diffraction analysis. The four analyzed compounds are structurally similar (*Tanimoto* index greater than 0.68, Table S2), differing by the substitution of the OCH_2CH_3 group at the *para* position of the aromatic ring 2 in compound **QC01** and the OCH_3 group in compound **QC02**. Compounds **QC03** and **QC04** feature chlorine (Cl) and bromine (Br) substitutions, respectively, also at the *para* position of aromatic ring 2 (Fig. 1). The compounds **QC01**, **QC02** and **QC04** crystallize in the monoclinic space group $P2_1/c$, with four molecules per unit cell and similar volumes (1977.0 (7) Å^3, 1835.8 (4) Å^3 and 1806.7 (5) Å^3, respectively). Compound **QC03** crystallizes in the triclinic space group $P\overline{1}$, with two molecules per unit cell and a smaller volume compared with **QC01**, **QC02** and **QC04** (Table 1).

The structural conformation of a molecule can be linked to its biological properties or activities, such as the planar conformation of chalcones, which has been described as having antifungal[80] and cytotoxic activities.[81] The presence of different substituents can result in distinct conformations for each molecule. To analyze these conformational differences, the four molecules were superimposed using the quinolinone core as an anchoring point. Molecules **CQ01** and **CQ02** have similar conformations; however, the presence of an OCH_2CH_3 group compared with an OCH_3 group causes a 7.08° difference in aromatic ring 2. Next, we observe the superimpositions of **CQ02** with **CQ04**, where the OCH_3 group compared with Br results in a 6.60° difference in aromatic ring 2. Furthermore, the superimposition of **CQ01** with **CQ04** shows a 13.48° difference in aromatic ring 2 owing to the presence of the OCH_2CH_3 group compared to Br. On the other hand, the **CQ03** molecule, which contains Cl, also shows conformational differences when compared with the others: **CQ03** with **CQ02** (Cl to OCH_3 – 7.08° in aromatic ring 1), **CQ03** with **CQ04** (Cl to Br – 20.18° in aromatic ring 1), and **CQ03** with **CQ01** (Cl to OCH_2CH_3 – 9.05° in aromatic ring 2) (Fig. 2). We observe that different substituents can lead to multiple conformations for each molecule. This variation can reflect the diverse intermolecular interactions and the specific supramolecular arrangement of each molecule, which can be directly linked to their physicochemical properties.

The supramolecular arrangement of **CQ01** is stabilized by C–H···O and C–H···π interactions, while **CQ02** is stabilized only by C–H···O interactions. For **CQ01**, the C20–H20···Cg3 interaction contributes to stability along (100) direction (Fig. 3c), C8–H8B···O1, C8–H8A···O1 and C12–H12···O3 interactions contribute along (010) direction

© 2025 The Author(s). *Biofuels, Bioproducts and Biorefining* published by Society of Industrial Chemistry and John Wiley & Sons Ltd.

19321031, 0, Downloaded from https://scijournals.onlinelibrary.wiley.com/doi/10.1002/bbb.2774 by Capes, Wiley Online Library on [28/08/2025]. See the Terms and Conditions (https://onlinelibrary.wiley.com/terms-and-conditions) on Wiley Online Library for rules of use; OA articles are governed by the applicable Creative Commons License

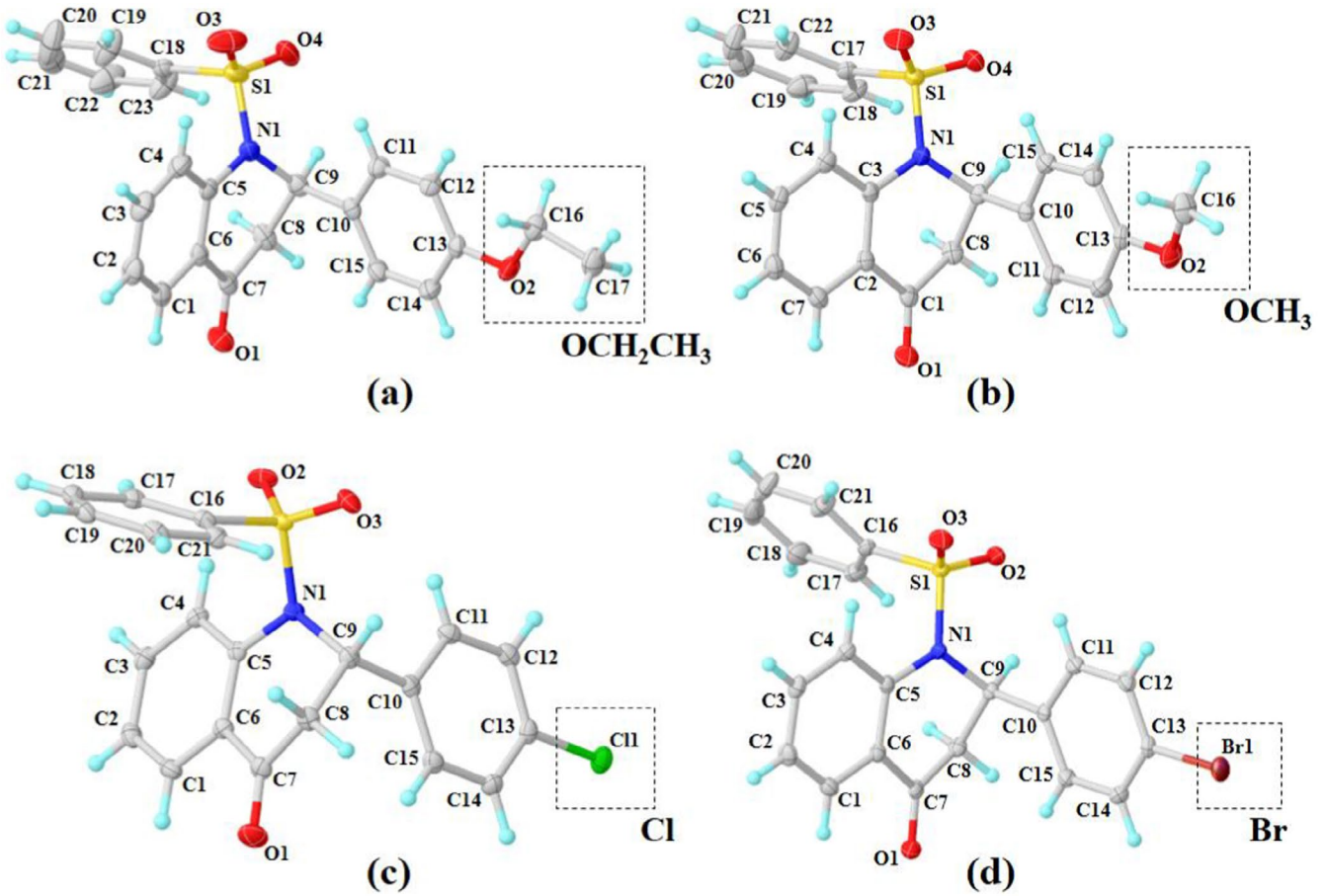

Figure 1. ORTEP representation for **QC01** (a), **QC02** (b), **QC03** (c) and **QC04** (d) with ellipsoids at 50% of probability.

(Fig. 3b), while C1–H1···O4 and C8–H8A···O4 interactions contribute to growth along (001) direction (Fig. 3a). For **CQ02**, C20–H20···O1 and C16–H16C···O1 interactions contribute to growth along (100) direction (Fig. 4a), while C8–H8A···O4, C8–H8B···O1 and C14–H14···O3 interactions contribute to growth along the (010) and (001) directions (Fig. 4b). Additionally, for **CQ03**, C15–H15···O1 and C14–H14···O1 interactions contribute to stability along the (100) direction (Fig. 5c) and C8–H8A···Cl1, C19–H19···Cl1 and C19–H19···O2 interaction contribute to growth along the (010) direction (Fig. 5a), while C1–H1···Cg1, C12–H12···O3 and C9–H9···O3 interactions contribute to growth along the (100) direction (Fig. 5b). For **CQ04**, C19–H19···O1 and C15–H15···Br1 interactions contribute to growth and stability along the (100) and (010) directions (Fig. 6a), while C8–H8A···O2, C8–H8B···O1 and C9–H9···O1 interactions contribute to growth along the (001) direction (Fig. 6b).

Note that, for the four compounds analyzed, the molecular arrangements are stabilized only by weak interactions (Table 2), but in the literature we find several authors describing these interactions as considerable for the stability of the supramolecular arrangement, in addition, several authors have linked certain interactions, such as C–H···π, to the enhancement of specific biological activities.[82–87] Additionally, C–H···O interactions have been identified as crucial for antibacterial targets[88] and for stabilizing complexes associated with antioxidant activity.[89]

The contacts were quantified by type through the two-dimensional 2D fingerprints obtained from Hirshfeld surfaces using CrystalExplorer software.[90] Hirshfeld surfaces are constructed based on electron density to determine regions of possible intermolecular interactions.[61,62] In constructing these surfaces, the distances from the internal atoms to the surface (d_i) and from the external atoms to the surface (d_e) are considered. These distances are incorporated into the equations that define the Hirshfeld surface, allowing for detailed visualization and analysis of intermolecular interactions.[61,62] The 2D fingerprints generated from the Hirshfeld surfaces show pseudo-mirrored peaks at 1.0 (d_e, d_i) – 1.2 (d_e, d_i), suggesting contacts involving hydrogen atoms (H···H). For all four compounds analyzed, these interactions are predominant owing to the organic nature of

© 2025 The Author(s). *Biofuels, Bioproducts and Biorefining* published by Society of Industrial Chemistry and John Wiley & Sons Ltd.

19321031, 0, Downloaded from https://scijournals.onlinelibrary.wiley.com/doi/10.1002/bbb.2774 by Capes, Wiley Online Library on [28/08/2025]. See the Terms and Conditions (https://onlinelibrary.wiley.com/terms-and-conditions) on Wiley Online Library for rules of use; OA articles are governed by the applicable Creative Commons License

Table 1. Crystallographic data and structure refinement for QC01, QC02, QC03 and QC04.

	QC01	QC02	QC03	QC04
Formula	$C_{23}H_{21}NO_4S$	$C_{22}H_{19}NO_4S$	$C_{21}H_{16}NO_3SCl$	$C_{21}H_{16}NO_3SBr$
Formula weight	407.47 g mol^{-1}	393.44 g mol^{-1}	397.86 g mol^{-1}	442.32 g mol^{-1}
Temperature	120 (2) K	120 (2) K	120 (2) K	120 (2) K
Wavelength	0.71073	0.71073 Å	0.71073 Å	0.71073 Å
Crystal system	Monoclinic	Monoclinic	Triclinic	Monoclinic
Space group, *Z*	$P2_1/c$, 4	$P2_1/c$, 4	$P\bar{1}$, 2	$P2_1/c$, 4
Unit cell dimensions	*a* = 9.884 (2) Å *b* = 23.047 (5) Å *c* = 8.8652 (18) Å α = 90° β = 101.763 (4)° γ = 90°	*a* = 10.0696 (14) Å *b* = 21.739 (3) Å *c* = 8.6674 (12) Å α = 90° β = 104.625 (2)° γ = 90°	*a* = 8.2750 (18) Å *b* = 10.011 (2) Å *c* = 11.853 (3) Å α = 65.602 (3)° β = 79.928 (3)° γ = 77.577 (3)°	*a* = 10.3865 (16) Å *b* = 19.972 (3) Å *c* = 8.9477 (14) Å α = 90° β = 103.249 (2)° γ = 90°
Volume	1977.0 (7) Å^3	1835.8 (4) Å^3	869.2 (3) Å^3	1806.7 (5) Å^3
Calculated density	1.369 g m^{-3}	1.424 g m^{-3}	1.520 g m^{-3}	1.626
Absorption coefficient	0.194 mm^{-1}	0.206 mm^{-1}	0.363 mm^{-1}	2.413 mm^{-1}
Goodness-of-fit (S)	1.027	1.008	1.039	1.050
Final *R* índices [I > 2σ(I)]	R_1 = 0.0520 wR_2 = 0.1164	R_1 = 0.0477 wR_2 = 0.0958	R_1 = 0.0322 wR_2 = 0.0792	R_1 = 0.0237 wR_2 = 0.0573
R indices (all data)	R_1 = 0.0783 wR_2 = 0.1311	R_1 = 0.0896 wR_2 = 0.1108	R_1 = 0.0398 wR_2 = 0.0833	R_1 = 0.0297 wR_2 = 0.0596

the molecules (**QC01**, 49.7%; **QC02**, 44.3%; **QC03**, 31.3%; and **QC04**, 32.3%) (Fig. 7). Peaks around 1.2–1.4 (d_e) with 1.2–1.4 (d_i) indicate non-classical interactions (C–H···O), which were identified by geometric parameters in all structures and quantified at around 22%, followed by C–H···π interactions with similar quantifications. For compound **QC03**, C–H···Cl interactions were quantified at 13.4%, and for **QC04**, interactions involving Br were quantified at 12.7%, corroborating the interactions described by geometric parameters. These interactions represented over 90% of the total structural stability for all molecules.

Molecular modeling analysis

The theoretical calculations through DFT were performed for both the conformations of the molecules in the solid state and the conformations of the molecules in the gas phase. These theoretical parameters provide a more comprehensive comparison of the relationship between the chemical structures of these quinolinone–chalcones and their properties.[91] The conformation of these molecules in different phases provides insights and can support future research as well as biological and industrial applications.[92] The representation of the LUMO and HOMO orbital arrangements for molecules **QC01**, **QC02**, **QC03** and **QC04** is shown for the solid state [Fig. 8 (a)] and for the gas phase [Fig. 8 (b)]. For the analyzed molecules, the HOMO orbital is characterized as the bonding orbital with nucleophilic properties, while the LUMO orbital is characterized as the antibonding orbital with electrophilic properties, with energy values indicated in the figure. The difference between these energy values (Egap) can be an important indicator of certain molecular properties, as higher Egap values may suggest greater kinetic stability, higher excitation energies, and lower chemical reactivity.[93] For the solid state, the Egap values are: **QC03** (657.40 kJ mol^{-1}) > **QC04** (655.59 kJ mol^{-1}) > **QC02** (623.74 kJ mol^{-1}) > **QC01** (615.60 kJ mol^{-1}), while for the gas phase: **QC03** (662.65 kJ mol^{-1}) > **QC04** (657.14 kJ mol^{-1}) > **QC02** (620.69 kJ mol^{-1}) > **QC01** (618.51 kJ mol^{-1}). Note that for both phases, the Egap values are similar, with **QC03** having the highest Egap and **QC01** the lowest.

The MEP map is an important physicochemical tool that contributes to predicting reactive sites targeted in chemical reactions. It was calculated for both the conformations of the molecules in the solid state and the conformations of the molecules in the gas phase (Fig. 9). The MEP map illustrates that the most negative region (color red) is situated on the oxygen atoms of the sulfonamide and carbonyl group (for both states, solid and gas phase) (Fig. 9). Additionally, positive regions (color blue) are close to the hydrogen atoms and the aromatic ring attached to the sulfonamide group. Based on the analysis of the MEP map and the interactions

© 2025 The Author(s). *Biofuels, Bioproducts and Biorefining* published by Society of Industrial Chemistry and John Wiley & Sons Ltd.

19321031, 0, Downloaded from https://scijournals.onlinelibrary.wiley.com/doi/10.1002/bbb.2774 by Capes, Wiley Online Library on [28/08/2025]. See the Terms and Conditions (https://onlinelibrary.wiley.com/terms-and-conditions) on Wiley Online Library for rules of use; OA articles are governed by the applicable Creative Commons License

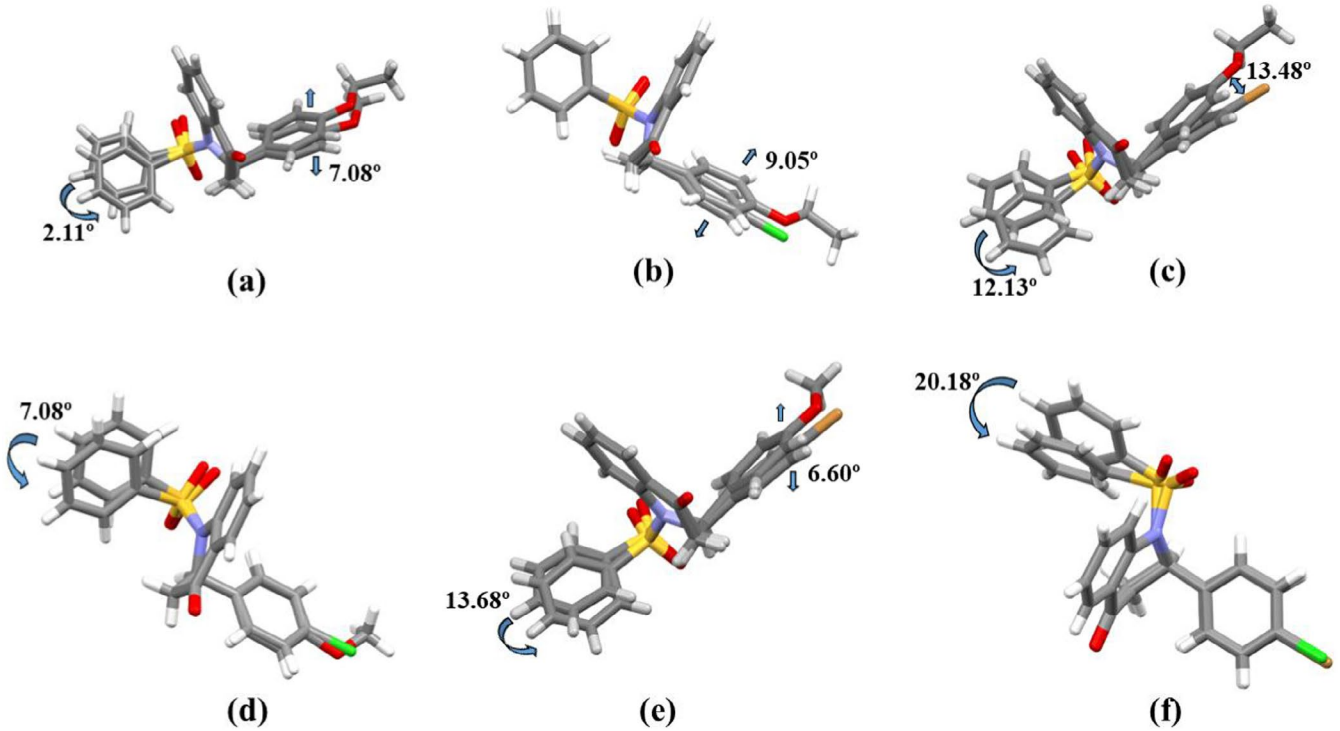

Figure 2. Overlap between compounds **CQ01** with **CQ02** (a), **CQ01** with **CQ03** (b), **CQ01** with **CQ04** (c), **CQ02** with **CQ03** (d), **CQ02** with **CQ04** (e), **CQ03** with **CQ04** (f).

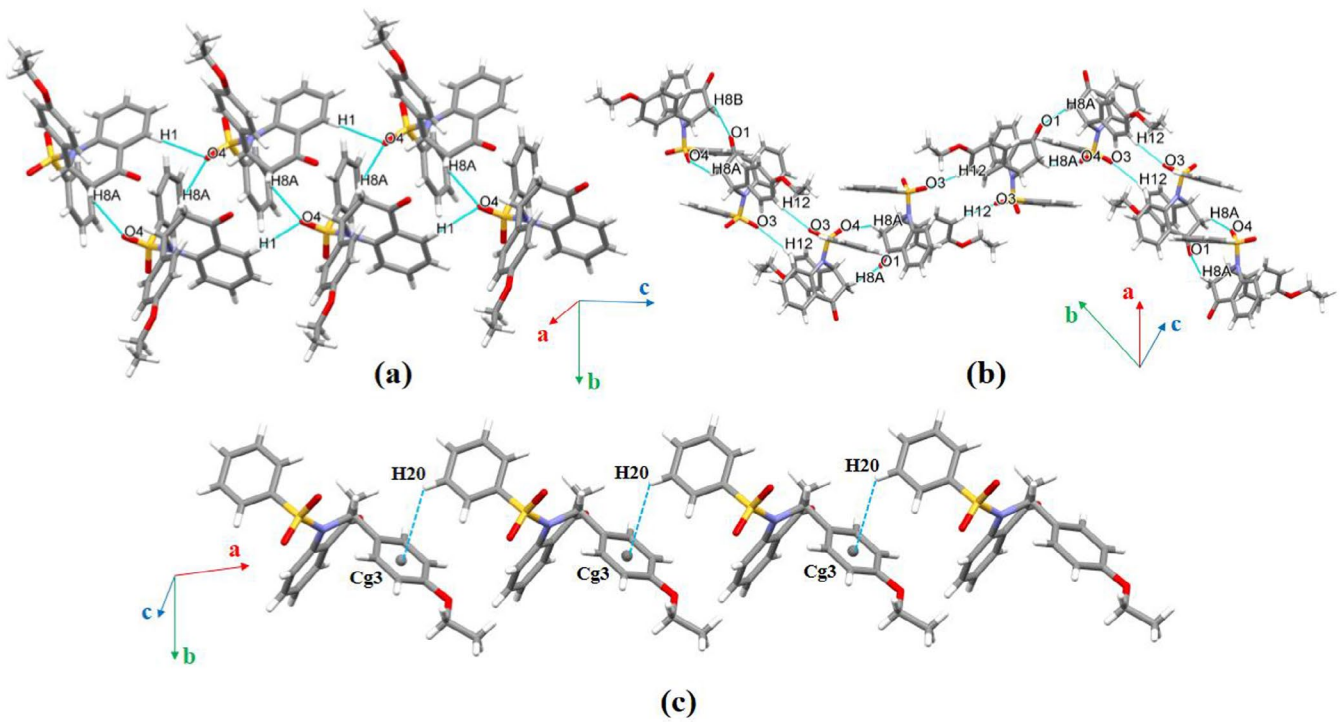

Figure 3. Representations for **QC01** interactions. C1–H1···O4 and C8–H8A···O4 interactions (a); C8–H8B···O1, C8–H8A···O4, C12–H12···O3, C8–H8A···O1 interactions (b); and C20–H20···Cg3 interaction (c). (a-axis (100); b-axis (010); c-axis (001)).

© 2025 The Author(s). *Biofuels, Bioproducts and Biorefining* published by Society of Industrial Chemistry and John Wiley & Sons Ltd.

19321031, 0, Downloaded from https://scijournals.onlinelibrary.wiley.com/doi/10.1002/bbb.2774 by Capes, Wiley Online Library on [28/08/2025]. See the Terms and Conditions (https://onlinelibrary.wiley.com/terms-and-conditions) on Wiley Online Library for rules of use; OA articles are governed by the applicable Creative Commons License

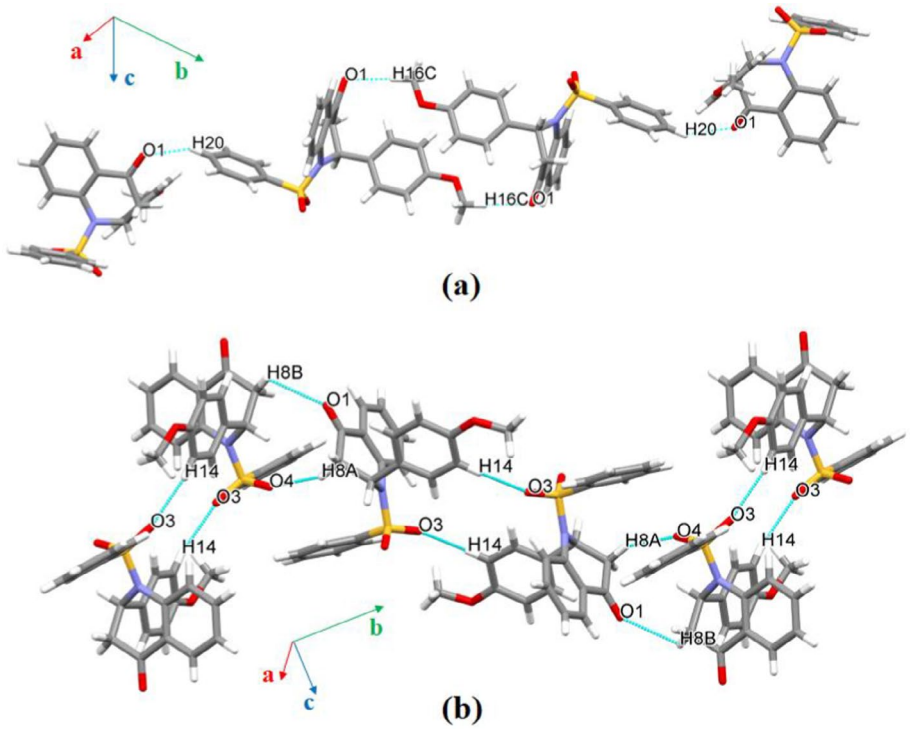

Figure 4. Representations for **QC02** interactions. C16–H16C···O1 and C20–H20···O1 interactions (a); C8–H8B···O1, C8–H8A···O4 and C14–H14···O3 interactions (b). (a-axis (100); b-axis (010); c-axis (001)).

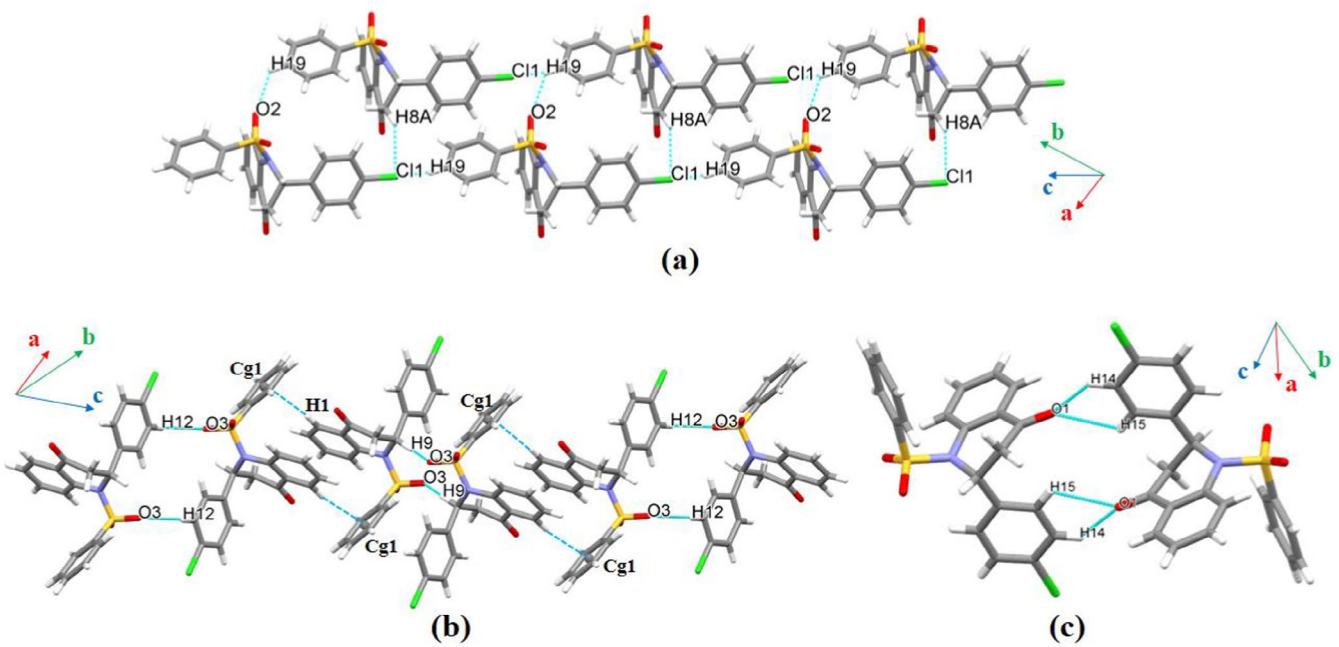

Figure 5. Representations for **QC03** interactions. C19–H19···O2, C8–H8A···Cl1 and C19–H19···Cl1 interactions (a); C1–H1···Cg1, C9–H9···O3 and C12–H12···O3 interactions (b); C14–H14···O1 and C15–H15···O1 interactions (c). (a-axis (100); b-axis (010); c-axis (001)).

© 2025 The Author(s). *Biofuels, Bioproducts and Biorefining* published by Society of Industrial Chemistry and John Wiley & Sons Ltd.

19321031, 0, Downloaded from https://scijournals.onlinelibrary.wiley.com/doi/10.1002/bbb.2774 by Capes, Wiley Online Library on [28/08/2025]. See the Terms and Conditions (https://onlinelibrary.wiley.com/terms-and-conditions) on Wiley Online Library for rules of use; OA articles are governed by the applicable Creative Commons License

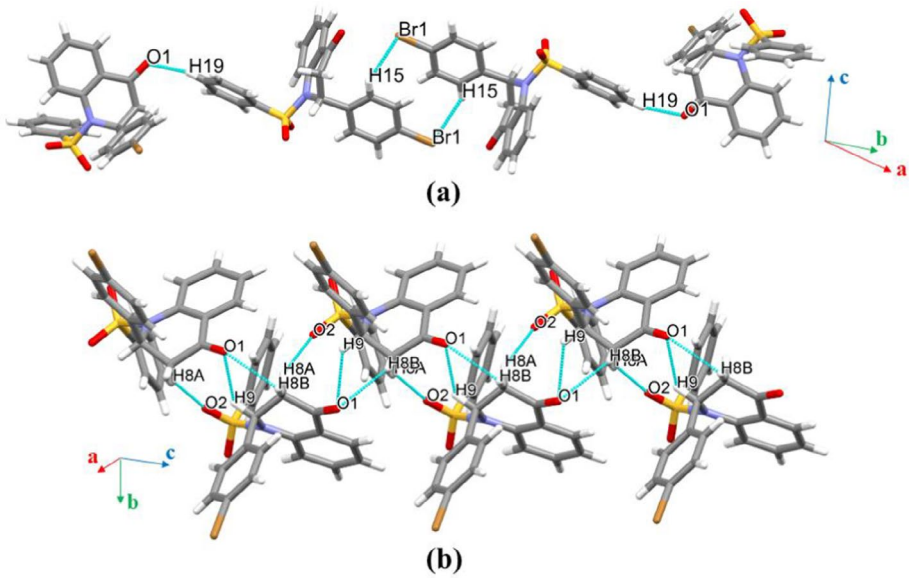

Figure 6. Representations for **QC04** interactions. C19–H19···O1 and C15–H15···Br1 interactions (a); C9–H9···O1, C8–H8B···O1 and C8–H8A···O2 interactions (b). (a-axis (100); b-axis (010); c-axis (001)).

Table 2. Molecular interactions for QC01, QC02, QC03 and QC04.

QC	Interaction	d (D–H) Å	d (H···A) Å	d (D–A) Å	d (D–H–A) (°)	Symmetry code
01	C1–H1···O4	0.950 (1)	2.707 (5)	3.337 (6)	124,41 (6)	*x*, *y*, –1+*z*
	C8–H8A···O4	0.990 (1)	2.683 (6)	3.534 (5)	144.16 (7)	*x*, 1/2–*y*, –1/2+*z*
	C8–H8B···O1	0.991 (1)	2.616 (6)	2.956 (6)	100.11 (5)	*x*, 1/2–*y*, –1/2+*z*
	C12–H12···O3	0.950 (1)	2.462 (5)	3.394 (5)	166.93 (5)	1–*x*, 1–*y*, –*z*
	C8–H8A···O1	0.990 (1)	2.662 (6)	2.956 (6)	97.32 (6)	*x*, 1/2–*y*, 1/2+*z*
	C20–H20···Cg3	0.950 (1)	3.375 (5)	4.019 (5)	127.04 (6)	1+*x*, *y*, *z*
02	C20–H20···O1	0.950 (1)	2.634 (6)	3.412 (5)	139.44 (6)	–1+*x*, 1/2–*y*, –1/2+*z*
	C16–H16C···O1	0.980 (1)	2.649 (6)	3.553 (6)	153.45 (5)	–*x*, 1–*y*, 1–*z*
	C8–H8B···O1	0.990 (1)	2.661 (5)	3.084 (5)	105.97 (6)	*x*, 1/2–*y*, –1/2+*z*
	C8–H8A···O4	0.990 (1)	2.527 (7)	3.437 (7)	152.82 (7)	*x*, 1/2–*y*, –1/2+*z*
	C14–H14···O3	0.950 (1)	2.447 (6)	3.328 (6)	154.25 (5)	1–*x*, 1–*y*, 2–*z*
03	C19–H19···O2	0.950 (1)	2.695 (4)	3.331 (4)	124.86 (7)	1+*x*, *y*, *z*
	C8–H8A···Cl1	0.990 (1)	2.896 (5)	3.772 (6)	147.93 (6)	1+*x*, *y*, *z*
	C19–H19···Cl1	0.950 (1)	2.891 (6)	3.467 (7)	120.12 (7)	–1+*x*, –1+*y*, *z*
	C14–H14···O1	0.950 (1)	2.648 (4)	3.252 (6)	121.97 (4)	1–*x*, –*y*, 1–*z*
	C15–H15···O1	0.950 (1)	2.691 (5)	3.279 (4)	120.67 (7)	1–*x*, –*y*, 1–*z*
	C12–H12···O3	0.950 (1)	2.672 (5)	3.590 (6)	162.76 (6)	–*x*, 1–*y*, –*z*
	C9–H9···O3	1.000 (1)	2.515 (6)	3.347 (7)	140.75 (7)	1–*x*, 1–*y*, –*z*
	C1–H1···Cg1	0.950 (1)	3.171 (7)	3.586 (6)	125.69 (6)	1–*x*, 1–*y*, 1–*z*
04	C19–H19···O1	0.950 (1)	2.469 (6)	3.323 (6)	149.61 (6)	–1+*x*, 1/2–*y*, –1/2+*z*
	C15–H15···Br1	0.950 (1)	3.353 (5)	3.664 (7)	101.61 (5)	2–*x*, 1–*y*, 1–*z*
	C8–H8A···O2	0.991 (1)	2.401 (4)	3.300 (7)	150.74 (5)	*x*, 1/2–*y*, –1/2+*z*
	C9–H9···O1	1.000 (1)	2.567 (5)	3.245 (6)	124.92 (6)	*x*, 1/2–*y*, –1/2+*z*
	C8–H8B···O1	0.990 (1)	2.659 (6)	3.082 (5)	105.93 (5)	*x*, 1/2–*y*, –1/2+*z*

© 2025 The Author(s). *Biofuels, Bioproducts and Biorefining* published by Society of Industrial Chemistry and John Wiley & Sons Ltd.

19321031, 0, Downloaded from https://scijournals.onlinelibrary.wiley.com/doi/10.1002/bbb.2774 by Capes, Wiley Online Library on [28/08/2025]. See the Terms and Conditions (https://onlinelibrary.wiley.com/terms-and-conditions) on Wiley Online Library for rules of use; OA articles are governed by the applicable Creative Commons License

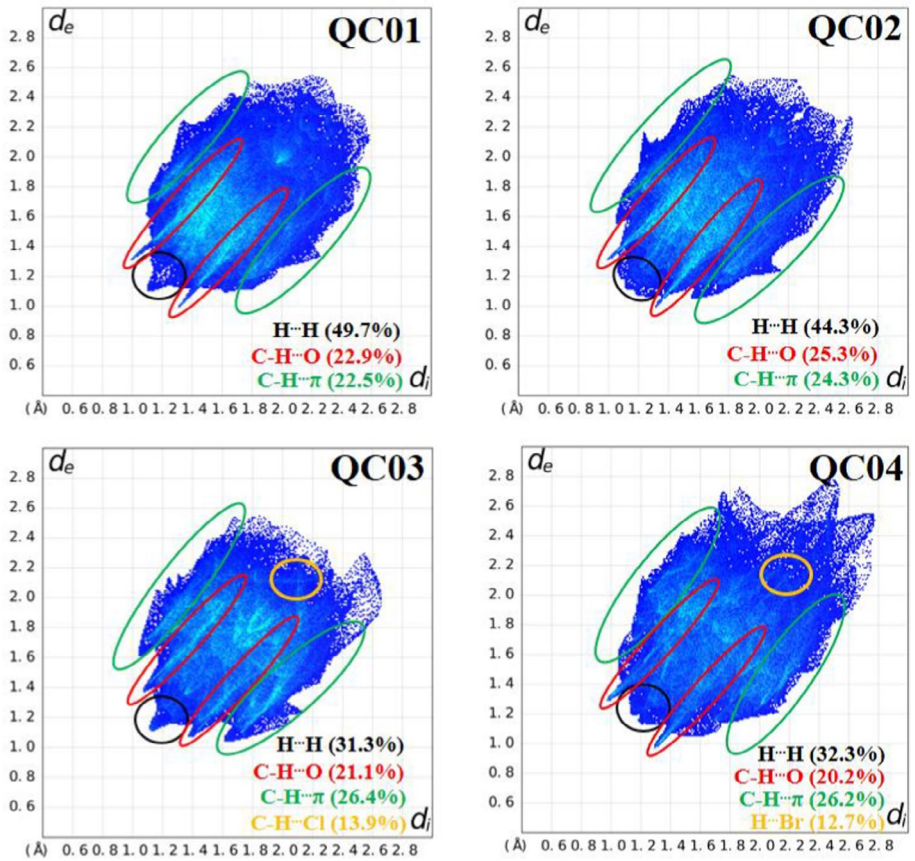

Figure 7. 2D Fingerprints with percentages of the contact types for **QC01**, **QC02**, **QC03** and **QC04**.

observed in the aromatic ring (attached to the sulfonamide group) in the crystal structures, the possibility of a nucleophilic attack occurring in this region can be suggested.

Machine learning analysis

The reaction rate constant (k_{OH}) is the main kinetic parameter for assessing a compound's degradation efficiency *via* hydroxyl radical attack, for which a high k_{OH} value indicates faster oxidation. Here, we examined the highest AD% values for the ML model (XGBoost) and molecular descriptor, with the MACCS fingerprint returning AD% values above 59% for all tested molecules. This suggests that MACCS provides more accurate predictions than the Morgan fingerprint using the *py*SiRC tool. Table 3 presents k_{OH} values for the main diesel component (1.14×10^{10} M^{-1} s^{-1}) and three biodiesel components – BD M9OD (5.94×10^{9} M^{-1} s^{-1}), BD MPAL (4.98×10^{9} M^{-1} s^{-1}) and BD M8OD (5.94×10^{9} M^{-1} s^{-1}), respectively.

Taking the **QC01**, **QC02**, **QC03** and **QC04** (this work) as the reference molecules, their molecular similarity was evaluated using the *Tanimoto* index,[77] calculated over the Morgan Fingerprint of 2048 bits[96] by using the RDKit,[97] against some target compounds, including the quinolinone–chalcones QC,[6] CQH,[95] arylsulfonamide chalcones NSC and HSC,[94] chalcones Chal01 and Chal05,[41] a tri-methoxy chalcone (TMC20)[45] and commercial additives (*CA: BHT, TBHQ, BHA, PG, PY and GA,[79] see Table S2 in the supplementary information). The lower similarity observed against the *CA is within 0.035–0.051 for the quinolinone derivatives with respect to BHT, and for our previous molecules is within 0.057–0.18 to TMC20. This was done focusing on biodiesel additive applications in standardized tests like Rancimat EN 15751:2014[98] and combustion heat (ASTM D4809).[99]

The values of k_{OH} for the quinolinone–chalcones in the present study are 6.73×10^{9} M^{-1} s^{-1} for **QC01**, 5.45×10^{9} M^{-1} s^{-1} for **QC02**, 4.89×10^{9} M^{-1} s^{-1} for **QC03**, and 7.97×10^{9} M^{-1} s^{-1} for **QC04**. These can be compared with oxidation rates previously published by our group,[6] ranging from a value, close to the present ones, of 7.44×10^{9} M^{-1} s^{-1}, to a k_{OH} equal to 1.07×10^{10} M^{-1} s^{-1} for the promising trimethoxy chalcone (TMC20).[45] Further comparision can be made to four arylsulfonamide chalcones, with k_{OH} equal to

© 2025 The Author(s). *Biofuels, Bioproducts and Biorefining* published by Society of Industrial Chemistry and John Wiley & Sons Ltd.

19321031, 0, Downloaded from https://scijournals.onlinelibrary.wiley.com/doi/10.1002/bbb.2774 by Capes, Wiley Online Library on [28/08/2025]. See the Terms and Conditions (https://onlinelibrary.wiley.com/terms-and-conditions) on Wiley Online Library for rules of use; OA articles are governed by the applicable Creative Commons License

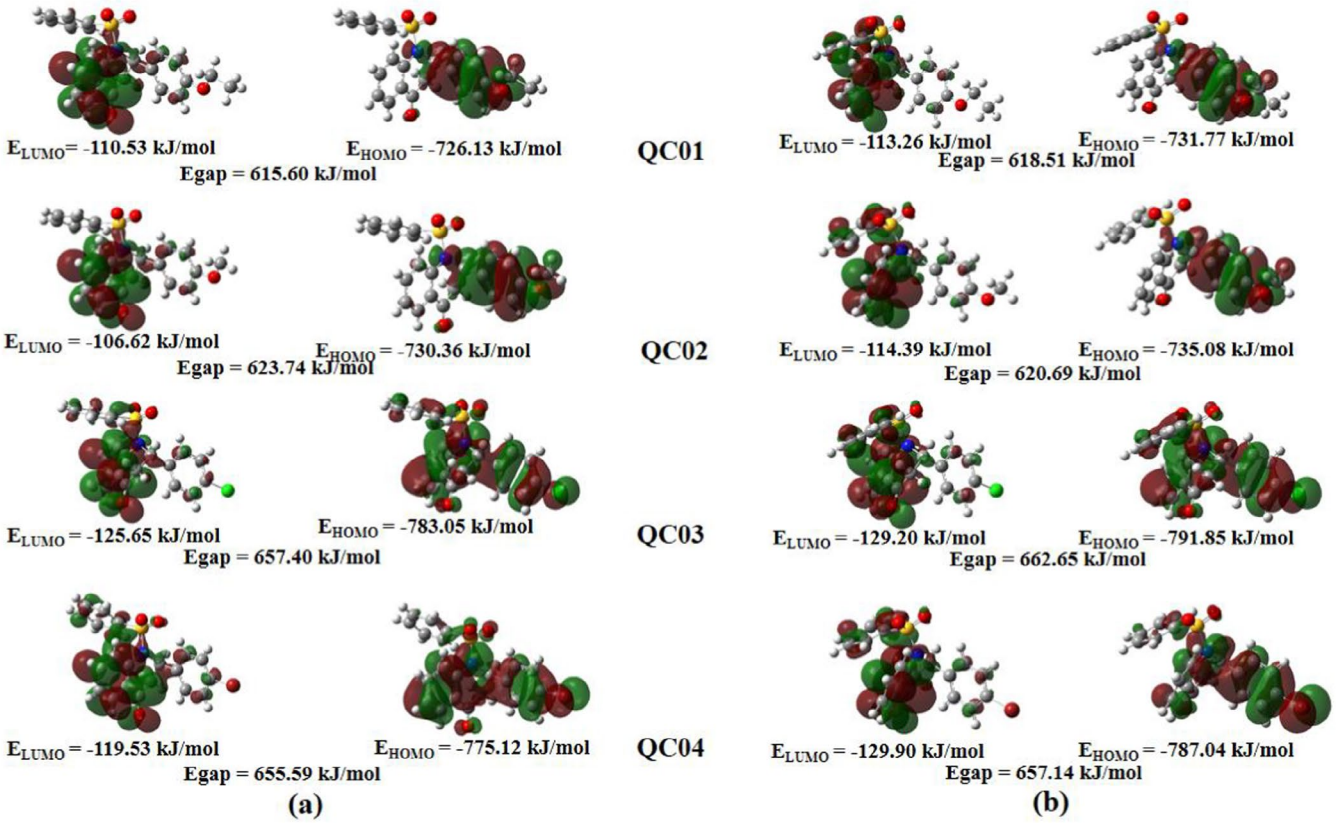

Figure 8. The frontier molecular orbitals orbitals for **QC01**, **QC02**, **QC03** and **QC04**. Solid state (a) and gas phase (b).

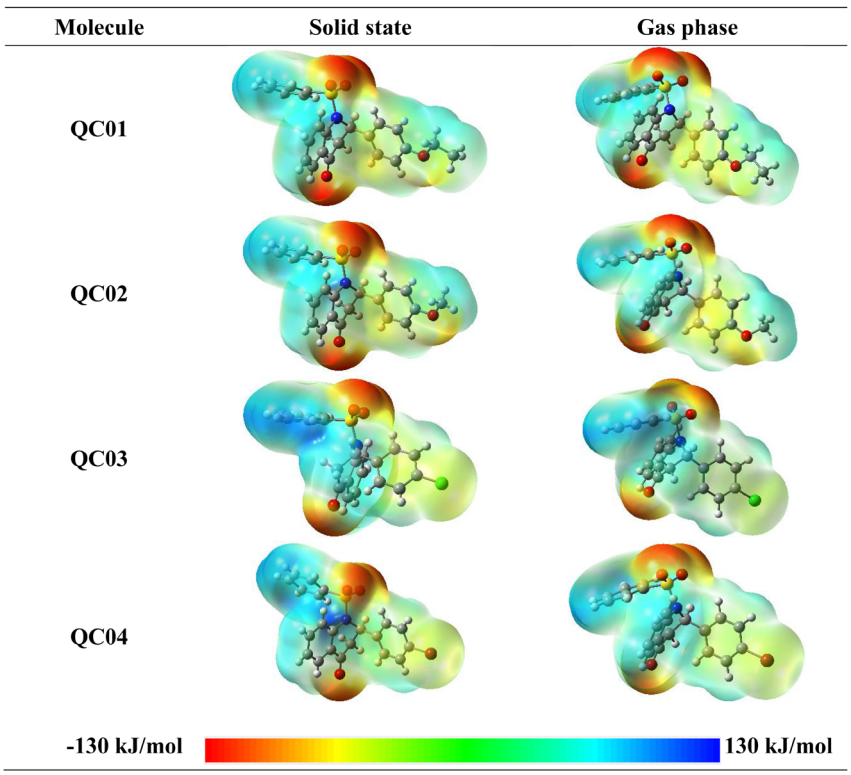

Figure 9. The MEP map surfaces for **QC01**, **QC02**, **QC03** and **QC04**.

© 2025 The Author(s). *Biofuels, Bioproducts and Biorefining* published by Society of Industrial Chemistry and John Wiley & Sons Ltd.

19321031, 0, Downloaded from https://scijournals.onlinelibrary.wiley.com/doi/10.1002/bbb.2774 by Capes, Wiley Online Library on [28/08/2025]. See the Terms and Conditions (https://onlinelibrary.wiley.com/terms-and-conditions) on Wiley Online Library for rules of use; OA articles are governed by the applicable Creative Commons License

Table 3. The reaction rate (k_{OH}) for the dihydroquinolin-4(1H)-one compounds QC01, QC02, QC03, QC04 (this work). Diesel and biodiesel (BD) are represented by their majority compound, respectively. Previously studied compounds, and other commercial additives (*CA). The values were obtained with the ML model XGBoost and separated into two types of molecular fingerprints Morgan and MACCS. AD is the percentage similarity within the applicability domain.

Molecule	Reaction rate coefficient (k_{OH}) ($M^{-1} s^{-1}$)				Reference
	Morgan	AD (%)	MACCS	AD (%)	
Diesel[78]	6.05×10^9	50	1.14×10^{10}	76.92	Duarte *et al.*[41]
BD M9OD[78]	5.90×10^9	48.21	5.94×10^9	85	Duarte *et al.*[41]
BD MPAL[78]	5.70×10^9	58.7	4.98×10^9	89.47	Duarte *et al.*[41]
BD M8OD[78]	5.90×10^9	40.32	5.94×10^9	85	Duarte *et al.*[41]
QC01	6.98×10^9	18.57	6.73×10^9	61.73	This work
QC02	7.51×10^9	21.88	5.45×10^9	66.23	This work
QC03	5.18×10^9	20.31	4.89×10^9	59.49	This work
QC04	4.33×10^9	20.63	7.97×10^9	59.49	This work
QC[6]	3.82×10^9	18.42	7.44×10^9	62.82	This work
NSC[94]	2.25×10^{10}	21.43	9.29×10^9	60.42	This work
HSC[94]	2.81×10^{10}	21.69	9.29×10^9	60.42	This work
CQH[95]	4.99×10^9	15.48	4.20×10^9	61.90	This work
Chal01[41]	4.60×10^{10}	20.29	1.06×10^{10}	70.31	Duarte *et al.*[41]
Chal05[41]	1.24×10^{10}	24	8.17×10^9	62.71	Duarte *et al.*[41]
TMC20[45]	9.40×10^9	33.93	1.07×10^{10}	80	Duarte *et al.*[41]
*CA BHT[79]	4.16×10^9	100	4.34×10^9	100	Duarte *et al.*[41]
*CA TBHQ[79]	7.57×10^9	100	7.63×10^9	100	Duarte *et al.*[41]
*CA BHA[79]	7.27×10^9	66.67	4.31×10^9	77.78	Duarte *et al.*[41]
*CA PG[79]	1.11×10^{10}	100	1.22×10^{10}	100	Duarte *et al.*[41]
*CA PY[79]	7.06×10^9	40.74	1.02×10^{10}	100	Duarte *et al.*[41]
*CA GA[79]	4.09×10^9	40.62	1.48×10^9	100	Duarte *et al.*[41]

1.06×10^{10} $M^{-1} s^{-1}$ for Chal01, to 8.17×10^9 $M^{-1} s^{-1}$ for Chal05,[41] to 8.17×10^9 $M^{-1} s^{-1}$ for both NSC and HSC.[94] Passing from TMC20 to Chal01, NSC, HSC, Chal05, **QC04**, QC and **QC01** the oxidation potential is decreasing, but always higher than or equivalent to those obtained for both diesel and BD reference molecules (Table 3).

The k_{OH} rate coefficients were also obtained for additive compounds, previously reported, with the higher values being observed, in increasing order, for TBHQ, 7.63×10^9 $M^{-1} s^{-1}$, PY, 1.02×10^{10} $M^{-1} s^{-1}$ and PG, 1.22×10^{10} $M^{-1} s^{-1}$, while values close to the ones in present work are observed for BHT, 4.34×10^9 $M^{-1} s^{-1}$, BHA 4.31×10^9 $M^{-1} s^{-1}$ alongside with 1.48×10^9 $M^{-1} s^{-1}$ for GA, which shows the lower oxidative potential (Table 3). Thus, the rate coefficients obtained for GA, BHT, BHA and CQH are even slightly below the reference molecules. These values suggest that oxidative degradation for the commercial additives (*CA), quinolinone–chalcones, tri-methoxi chalcone and arylsulfonamide chalcones, ordered by decreasing oxidation potential (PG > TMC20 > Chal01 > PY > NSC and HSC > Chal05 > **QC04**, QC and **QC01**), is higher than for diesel and biodiesel references. This aligns with experimental results through the Rancimat method reported by the authors.[41,45] Compared with existing additives, these oxidative rates are generally similar, suggesting that quinolinone–chalcone derivatives could be promising candidates to slow biodiesel degradation, suitable for enhancing its oxidative stability.

All these results indicate the potential of these compounds as possible additives; however, some aspects still need to be addressed and further investigated. The addition of antioxidants to biodiesel can enhance its oxidative stability, reducing the formation of harmful byproducts and extending its shelf life, which would minimize pollutant emissions and logistical costs.[100,101] However, considering environmental factors, the biodegradability and toxicity of additives must be carefully evaluated to prevent negative impacts. From an economic perspective, effective additives would increase

© 2025 The Author(s). *Biofuels, Bioproducts and Biorefining* published by Society of Industrial Chemistry and John Wiley & Sons Ltd.

19321031, 0, Downloaded from https://scijournals.onlinelibrary.wiley.com/doi/10.1002/bbb.2774 by Capes, Wiley Online Library on [28/08/2025]. See the Terms and Conditions (https://onlinelibrary.wiley.com/terms-and-conditions) on Wiley Online Library for rules of use; OA articles are governed by the applicable Creative Commons License

the commercial viability of biodiesel and diesel (which can contain biodiesel additives according to national regulations) while also reducing storage losses.[102] Furthermore, their compatibility with existing infrastructure is crucial to avoiding high adaptation costs, given that biodiesel can be used in diesel cycle engines with certain modifications.[100] Thus, the development of sustainable and cost-effective additives can make biodiesel more competitive and strengthen its adoption in the global energy matrix.

Conclusions

This work presented the synthesis and characterization of four new quinolinone–chalcone derivatives (**QC01**, **QC02**, **QC03** and **QC04**), demonstrating their potential applications as antioxidant additives in biofuels. These compounds are unprecedented in the literature, ensuring originality in their application as additives. Structural and supramolecular analyses revealed that different substitutions (Br, Cl, OCH_3 and OCH_2CH_3) on the quinolinone–chalcone influence intermolecular interactions. Specifically, C–H · O and C–H · π interactions were found to contribute significantly to the stability of the crystalline structures, and these interactions are consistent with previously reported biological activities in the literature. Additionally, theoretical calculations based on DFT for both solid and gas phases provided detailed insights into the distribution of molecular orbitals and their corresponding energies. **QC03** was found to have the highest Egap, suggesting greater kinetic stability, while **QC01** exhibited the lowest Egap, reflecting higher chemical reactivity.

Reaction rate coefficients (k_{OH}) showed that the studied compounds are effective in scavenging hydroxyl radicals, with **QC04** standing out by displaying a k_{OH} value comparable with those of commercial antioxidants such as BHT. Therefore, the quinolinone–chalcone derivatives synthesized in this study are promising candidates for slowing down oxidative degradation in biofuels. Future research could explore the detailed mechanisms of their antioxidant action and further evaluate the experimental aspects of these compounds, aiming at their application as biofuel additives.

Acknowledgements

The authors thank the Fundação de Amparo à Pesquisa do Estado de Goiás (FAPEG: 202310267000442, LRA/HBN), Coordenação de Aperfeiçoamento de Pessoal de Nível Superior and Conselho Nacional de Desenvolvimento Científico e Tecnológico (401425/2023-1 LRA/HBN). Theoretical calculations were performed in the High-Performance Computing Center of the Universidade Estadual de Goias. The Article Processing Charge for the publication of this research was funded by the Coordenação de Aperfeiçoamento de Pessoal de Nível Superior - Brasil (CAPES) (ROR identifier: 00x0ma614).

Conflict of interest statement

The authors declare no conflicts of interest.

References

1. Jurd L, Benson M and Wong R, New quinolinone and bis-quinolinone alkaloids from *Euxylophora paraensis*. *Aust J Chem* **36**(4):759 (1983). https://doi.org/10.1071/CH9830759.
2. Shiro T, Fukaya T and Tobe M, The chemistry and biological activity of heterocycle-fused quinolinone derivatives: a review. *Eur J Med Chem* **97**:397–408 (2015). https://doi.org/10.1016/j.ejmech.2014.12.004.
3. Chu X-M, Wang C, Liu W, Liang L-L, Gong K-K, Zhao C-Y *et al.*, Quinoline and quinolone dimers and their biological activities: an overview. *Eur J Med Chem* **161**:101–117 (2019). https://doi.org/10.1016/j.ejmech.2018.10.035.
4. Kaur P, A, Chandra A, Tanwar T, Sahu SK and Mittal A, Emerging quinoline- and quinolone-based antibiotics in the light of epidemics. *Chem Biol Drug Des* **100**(6):765–785 (2022). https://doi.org/10.1111/cbdd.14025.
5. Barr SA, Neville CF, Grundon MF, Boyd DR, Malone JF and Evans TA, Quinolinone cycloaddition as a potential synthetic route to dimeric quinoline alkaloids. *J Chem Soc, Perkin Trans 1* **4**:445 (1995). https://doi.org/10.1039/p19950000445.
6. Duarte VS, Paula RLG, Custodio JMF, D'Oliveira GDC, Borges LL, Pérez CN *et al.*, A new quinolinone-chalcone hybrid with potential antibacterial and herbicidal properties using in silico approaches. *J Mol Model* **28**(6):176 (2022). https://doi.org/10.1007/s00894-022-05140-9.
7. Othman ES, Hassan H and Abass M, Substituted quinolinones. 31. Some new Pyrano[3,2-c]quinoline-3-carboxamides and their antioxidant activity. *J Heterocyclic Chem* **56**(12):3257–3266 (2019). https://doi.org/10.1002/jhet.3721.
8. Hassan MM, Abdel-Kariem SM and Ali TE, Synthesis and antioxidant properties of some novel 1,3,4,2-oxadiaza phosphepino[6,7-c]quinolinones and pyrazolo[3,4:4′,3′] Quinolino[5,1-c][1,4,2]oxazaphosphinine. *Phosphorus Sulfur Silicon Relat Elem* **192**(7):866–873 (2017). https://doi.org/10.1080/10426507.2017.1290625.
9. Subashini R, Angajala G, Aggile K and Nawaz Khan F, Microwave-assisted solid acid-catalyzed synthesis of quinolinyl quinolinones and evaluation of their antibacterial, antioxidant activities. *Res Chem Intermed* **41**(7):4899–4912 (2015). https://doi.org/10.1007/s11164-014-1575-z.
10. Savegnago L, Vieira AI, Seus N, Goldani BS, Castro MR, Lenardão EJ *et al.*, Synthesis and antioxidant properties of novel quinoline–chalcogenium compounds. *Tetrahedron Lett* **54**(1):40–44 (2013). https://doi.org/10.1016/j.tetlet.2012.10.067.
11. Zhang Y, Fang Y, Liang H, Wang H, Hu K, Liu X *et al.*, Synthesis and antioxidant activities of 2-oxo-quinoline-3-carbaldehyde Schiff-base derivatives. *Bioorg Med Chem Lett* **23**(1):107–111 (2013). https://doi.org/10.1016/j.bmcl.2012.11.006.

© 2025 The Author(s). *Biofuels, Bioproducts and Biorefining* published by Society of Industrial Chemistry and John Wiley & Sons Ltd.

19321031, 0, Downloaded from https://scijournals.onlinelibrary.wiley.com/doi/10.1002/bbb.2774 by Capes, Wiley Online Library on [28/08/2025]. See the Terms and Conditions (https://onlinelibrary.wiley.com/terms-and-conditions) on Wiley Online Library for rules of use; OA articles are governed by the applicable Creative Commons License

12. Kumar M, Sharma K, Rajawat A, Khandelwal S and Samarth RM, Synthesis and evaluation of antioxidant and radical scavenging activities of quinolinobenzothiazinones. *Res Chem Intermed* **41**(4):2265–2276 (2015). https://doi.org/10.1007/s11164-013-1344-4.
13. Shankerrao S, Bodke YD and Mety SS, Synthesis, antioxidant, and antibacterial studies of phenolic esters and amides of 2-(1-Benzofuran-2-Yl) quinoline-4-carboxylic acid. *Med Chem Res* **22**(3):1163–1171 (2013). https://doi.org/10.1007/s00044-012-0117-8.
14. Hassan MM and Hassanin HM, An efficient new route for the synthesis of some 3-Hterocyclylquinolinones via novel 3-(1,2-Dihydro-4-hydroxy-1-methyl-2-oxoquinolin-3-yl)-3-oxopropanal and their antioxidant screening. *J Heterocyclic Chem* **54**(6):3321–3330 (2017). https://doi.org/10.1002/jhet.2952.
15. Abdel-Kader D and Talaat N, Ring transformation reactions of 4-hydroxy-3-nitro-6-phenyl-6 H -pyrano[3,2-c]quinoline-2,5-dione and antioxidant activity. *Synth Commun* **53**(5):376–385 (2023). https://doi.org/10.1080/00397911.2023.2175693.
16. Chu DTW, Claiborne AK, Clement JJ and Plattner JJ, Syntheses and antibacterial activity of novel 6-fluoro-7-(gem-disubstituted piperazin-1-Yl)-quinolines. *Can J Chem* **70**(5):1328–1337 (1992). https://doi.org/10.1139/v92-171.
17. Duraipandiyan V and Ignacimuthu S, Antibacterial and antifungal activity of flindersine isolated from the traditional medicinal plant, *Toddalia asiatica* (L.) Lam. *J Ethnopharmacol* **123**(3):494–498 (2009). https://doi.org/10.1016/j.jep.2009.02.020.
18. Hussein MF, Ismail MA and El-Adly RA, Synthesis and evaluation of 4-hydroxy quinolinone derivatives as antioxidants of lubricating grease. *IJOC* **6**(4):207–219 (2016). https://doi.org/10.4236/ijoc.2016.64021.
19. Senerovic L, Opsenica D, Moric I, Aleksic I, Spasić M and Vasiljevic B, Quinolines and quinolones as antibacterial, antifungal, anti-virulence, antiviral and anti-parasitic agents, in *Advances in Microbiology, Infectious Diseases and Public Health*, Vol. **1282**, ed. by Donelli G. Springer International Publishing, Cham, pp. 37–69 (2019). https://doi.org/10.1007/5584_2019_428.
20. Cheng G, Hao H, Dai M, Liu Z and Yuan Z, Antibacterial action of quinolones: from target to network. *Eur J Med Chem* **66**:555–562 (2013). https://doi.org/10.1016/j.ejmech.2013.01.057.
21. Jayagobi M, Raghunathan R, Sainath S and Raghunathan M, Synthesis and antibacterial property of pyrrolopyrano quinolinones and pyrroloquinolines. *Eur J Med Chem* **46**(6):2075–2082 (2011). https://doi.org/10.1016/j.ejmech.2011.02.060.
22. Subashini R and Khan F-RN, Solvent-free synthesis and antibacterial studies of some quinolinones. *Monatsh Chem* **143**(3):485–489 (2012). https://doi.org/10.1007/s00706-011-0608-1.
23. Naeem A, Badshah S, Muska M, Ahmad N and Khan K, The current case of quinolones: synthetic approaches and antibacterial activity. *Molecules* **21**(4):268 (2016). 10.3390 mol^{-1}ecules21040268.
24. Prasoona G, Kishore B and Brahmeshwari G, Synthesis and antimicrobial evaluation of benzimidazolyl pyrimido [4, 5- b] quinolinones. *LOC* **18**(4):303–310 (2021). https://doi.org/10.2174/1570178617999200602151152.
25. Hassanin HM, Ibrahim MA and Alnamer YA-S, Synthesis and antimicrobial activity of some novel 4-hydroxyquinolin-2(1H)-ones and Pyrano[3,2-c] quinolinones from 3-(1-Ethy1-4-Hydroxy-2-Oxo-1,2-Dihydroquinolin-3-Yl)-3-Oxopropanoic acid. *Turk J Chem* **36**:682–699 (2012). https://doi.org/10.3906/kim-1111-14.
26. Yaakob Z, Narayanan BN, Padikkaparambil S, Unni KS and Akbar PM, A review on the oxidation stability of biodiesel. *Renew Sust Energ Rev* **35**:136–153 (2014). https://doi.org/10.1016/j.rser.2014.03.055.
27. Pullen J and Saeed K, An overview of biodiesel oxidation stability. *Renew Sust Energ Rev* **16**(8):5924–5950 (2012). https://doi.org/10.1016/j.rser.2012.06.024.
28. Liu Y, Cruz-Morales P, Zargar A, Belcher MS, Pang B, Englund E *et al*., Biofuels for a sustainable future. *Cell* **184**(6):1636–1647 (2021). https://doi.org/10.1016/j.cell.2021.01.052.
29. Mishra VK and Goswami R, A review of production, properties and advantages of biodiesel. *Biofuels* **9**(2):273–289 (2018). https://doi.org/10.1080/17597269.2017.1336350.
30. Coyle W, The future of biofuels: a global perspective. *J Rural Ment Health* **32**(2):80–89 (2008). https://doi.org/10.1037/h0095952.
31. Fulton LM, Lynd LR, Körner A, Greene N and Tonachel LR, The need for biofuels as part of a low carbon energy future. *Biofuels Bioprod Biorefin* **9**(5):476–483 (2015). https://doi.org/10.1002/bbb.1559.
32. Jose TK and Anand K, Effects of biodiesel composition on its long term storage stability. *Fuel* **177**:190–196 (2016). https://doi.org/10.1016/j.fuel.2016.03.007.
33. Kumar N, Oxidative stability of biodiesel: causes, effects and prevention. *Fuel* **190**:328–350 (2017). https://doi.org/10.1016/j.fuel.2016.11.001.
34. Mittelbach M and Schober S, The influence of antioxidants on the oxidation stability of biodiesel. *J Am Oil Chem Soc* **80**(8):817–823 (2003). https://doi.org/10.1007/s11746-003-0778-x.
35. Haider K, Haider MR, Neha K and Yar MS, Free radical scavengers: an overview on heterocyclic advances and medicinal prospects. *Eur J Med Chem* **204**:112607 (2020). https://doi.org/10.1016/j.ejmech.2020.112607.
36. Bocchini B, Goldani B, Sousa FSS, Birmann PT, Brüning CA, Lenardão EJ *et al*., Synthesis and antioxidant activity of new selenium-containing quinolines. *Med Chem* **17**(6):667–676 (2021). https://doi.org/10.2174/1573406416666200403081831.
37. Atpadkar PP, Gopavaram S and Chaudhary S, *Natural–Product–Inspired Bioactive Alkaloids Agglomerated with Potential Antioxidant Activity: Recent Advancements on Structure-Activity Relationship Studies and Future Perspectives. Vitamins and Hormones*, Vol. **121**. Elsevier, Amsterdam, pp. 355–393 (2023). https://doi.org/10.1016/bs.vh.2022.10.002.
38. Varatharajan K and Pushparani DS, Screening of antioxidant additives for biodiesel fuels. *Renew Sust Energ Rev* **82**:2017–2028 (2018). https://doi.org/10.1016/j.rser.2017.07.020.
39. Ahmadi S, Abdolmaleki A and Jebeli Javan M, *In Silico Study of Natural Antioxidants. Vitamins and Hormones*, Vol. **121**. Elsevier, Amsterdam, pp. 1–43 (2023). https://doi.org/10.1016/bs.vh.2022.09.001.
40. Berneira LM, Rockembach CT, Da Silva CC, De Freitas SC, Rosa BN, Pinto E *et al*., Employment of thermal analysis applied to the oxidative stability evaluation of biodiesel using chalcone analogues. *J Therm Anal Calorim* **146**(4):1473–1482 (2021). https://doi.org/10.1007/s10973-020-10189-w.
41. Duarte VS, Borges D, D'Oliveira GDC, Faria ECM, De Almeida LR, Carvalho-Silva VH *et al*., Arylsulfonamide chalcones as alternatives for fuel additives: antioxidant

© 2025 The Author(s). *Biofuels, Bioproducts and Biorefining* published by Society of Industrial Chemistry and John Wiley & Sons Ltd.

19321031, 0, Downloaded from https://scijournals.onlinelibrary.wiley.com/doi/10.1002/bbb.2774 by Capes, Wiley Online Library on [28/08/2025]. See the Terms and Conditions (https://onlinelibrary.wiley.com/terms-and-conditions) on Wiley Online Library for rules of use; OA articles are governed by the applicable Creative Commons License

activity and machine learning protocol studies. *New J Chem* **47**(21):10003–10015 (2023). https://doi.org/10.1039/D3NJ00255A.
42. Sallum LO, Duarte VS, Custodio JMF, Faria ECM, Da Silva AM, Lima RS *et al*., Cyclohexanone-based chalcones as alternatives for fuel additives. *ACS Omega* **7**(14):11871–11886 (2022). https://doi.org/10.1021/acsomega.1c07333.
43. Faria ECM, Duarte VS, De Paula RLG, Da Silva AM, Fernandes FS, Vaz WF *et al*., Comparative study of chalcones and their potential as additives for biofuels. *Energy Fuel* **35**(1):552–560 (2021). https://doi.org/10.1021/acs.energyfuels.0c03448.
44. Da Silva CC, Pacheco BS, De Freitas SC, Berneira LM, Dos Santos MAZ, Pizzuti L *et al*., Hydroxychalcones: synthetic alternatives to enhance oxidative stability of biodiesel, in *Increased Biodiesel Efficiency*, ed. by Trindade M. Springer International Publishing, Cham, pp. 81–110 (2018). https://doi.org/10.1007/978-3-319-73552-8_4.
45. Moreira CA, Faria ECM, Queiroz JE, Duarte VS, Gomes MDN, Da Silva AM *et al*., Structural insights and antioxidant analysis of a tri-methoxy chalcone with potential as a diesel-biodiesel blend additive. *Fuel Process Technol* **227**:107122 (2022). https://doi.org/10.1016/j.fuproc.2021.107122.
46. Chen T and Guestrin C, *XGBoost: A Scalable Tree Boosting System. In Proceedings of the 22nd ACM SIGKDD International Conference on Knowledge Discovery and Data Mining*. ACM, San Francisco, CA, USA, pp. 785–794 (2016). https://doi.org/10.1145/2939672.2939785.
47. Jung J, Moon J-O, Ahn SI and Lee H, Predicting antioxidant activity of compounds based on chemical structure using machine learning methods. *Korean J Physiol Pharmacol* **28**(6):527–537 (2024). https://doi.org/10.4196/kjpp.2024.28.6.527.
48. Sanches-Neto FO, Dias-Silva JR, Keng Queiroz Junior LH and Carvalho-Silva VH, "PySiRC": machine learning combined with molecular fingerprints to predict the reaction rate constant of the radical-based oxidation processes of aqueous organic contaminants. *Environ Sci Technol* **55**(18):12437–12448 (2021). https://doi.org/10.1021/acs.est.1c04326.
49. Castro MRCD, Aragão ÂQ, Silva CCD, Perez CN, Queiroz DPK, Queiroz Júnior LHK *et al*., Conformational variability in sulfonamide chalcone hybrids: crystal structure and cytotoxicity. *J Braz Chem Soc* **27** (2015). https://doi.org/10.5935/0103-5053.20150341.
50. De Castro MRC, Naves RF, Bernardes A, Da Silva CC, Perez CN, Moura AF *et al*., Tandem chalcone-sulfonamide hybridization, cyclization and further Claisen–Schmidt condensation: tuning molecular diversity through reaction time and order and catalyst. *Arab J Chem* **13**(1):1345–1354 (2020). https://doi.org/10.1016/j.arabjc.2017.11.005.
51. D'Oliveira GDC, Moura A, De Moraes M, Perez C and Lião L, Synthesis, characterization and evaluation of in vitro antitumor activities of novel chalcone-quinolinone hybrid compounds. *J Braz Chem Soc* **29** (2018). https://doi.org/10.21577/0103-5053.20180108.
52. Kim JH, Ryu HW, Shim JH, Park KH and Withers SG, Development of new and selective Trypanosoma Cruzi trans-sialidase inhibitors from sulfonamide chalcones and their derivatives. *Chembiochem* **10**(15):2475–2479 (2009). https://doi.org/10.1002/cbic.200900108.
53. Custodio JMF, Gotardo F, Vaz WF, D'Oliveira GDC, De Almeida LR, Fonseca RD *et al*., Benzenesulfonyl incorporated chalcones: synthesis, structural and optical properties. *J Mol Struct* **1208**:127845 (2020). https://doi.org/10.1016/j.molstruc.2020.127845.
54. Gomes M, Muratov E, Pereira M, Peixoto J, Rosseto L, Cravo P *et al*., Chalcone derivatives: promising starting points for drug design. *Molecules* **22**(8):1210 (2017). 10.3390 mol^{-1}ecules22081210.
55. Katsuno K, Burrows JN, Duncan K, Van Huijsduijnen RH, Kaneko T, Kita K *et al*., Hit and Lead criteria in drug discovery for infectious diseases of the developing world. *Nat Rev Drug Discov* **14**(11):751–758 (2015). https://doi.org/10.1038/nrd4683.
56. Sweeting SG, Hall CL, Potticary J, Pridmore NE, Warren SD, Cremeens ME *et al*., The solubility and stability of heterocyclic chalcones compared with Trans -chalcone. *Acta Crystallogr Sect B: Struct Sci Cryst Eng Mater* **76**(1):13–17 (2020). https://doi.org/10.1107/S2052520619015907.
57. Sheldrick GM, A short history of SHELX. *Acta Crystallogr Sect A Found Crystallogr* **64**(1):112–122 (2008). https://doi.org/10.1107/S0108767307043930.
58. Dolomanov OV, Bourhis LJ, Gildea RJ, Howard JAK and Puschmann H, OLEX2: a complete structure solution, refinement and analysis program. *J Appl Cryst* **42**(2):339–341 (2009). https://doi.org/10.1107/S0021889808042726.
59. Groom CR, Bruno IJ, Lightfoot MP and Ward SC, The Cambridge structural database. *Acta Crystallogr Sect B: Struct Sci Cryst Eng Mater* **72**(2):171–179 (2016). https://doi.org/10.1107/S2052520616003954.
60. Macrae CF, Bruno IJ, Chisholm JA, Edgington PR, McCabe P, Pidcock E *et al*., Mercury CSD 2.0 – new features for the visualization and investigation of crystal structures. *J Appl Crystallogr* **41**(2):466–470 (2008). https://doi.org/10.1107/S0021889807067908.
61. Spackman MA and Jayatilaka D, Hirshfeld surface analysis. *CrystEngComm* **11**(1):19–32 (2009). https://doi.org/10.1039/B818330A.
62. McKinnon JJ, Jayatilaka D and Spackman MA, Towards quantitative analysis of intermolecular interactions with Hirshfeld surfaces. *Chem Commun* **37**:3814 (2007). https://doi.org/10.1039/b704980c.
63. McKinnon JJ, Mitchell AS and Spackman MA, Hirshfeld surfaces: a new tool for Visualising and exploring molecular crystals. *Chem Eur J* **4**(11):2136–2141 (1998). https://doi.org/10.1002/(SICI)1521-3765(19981102)4:11<2136::AID-CHEM2136>3.0.CO;2-G.
64. Spackman MA and McKinnon JJ, Fingerprinting intermolecular interactions in molecular crystals. *CrystEngComm* **4**(66):378–392 (2002). https://doi.org/10.1039/B203191B.
65. Burke K, Perspective on density functional theory. *J Chem Phys* **136**(15):150901 (2012). https://doi.org/10.1063/1.4704546.
66. Frisch MJ, Trucks GW, Schlegel HB, Scuseria GE, Robb MA, Cheeseman JR *et al*., *Gaussian 09, Revision A.02*. Gaussian Inc, Wallingford, CT (2016).
67. Wiberg KB, Basis set effects on calculated geometries: 6-311++G** vs. aug-cc-pVDZ. *J Comput Chem* **25**(11):1342–1346 (2004). https://doi.org/10.1002/jcc.20058.
68. Hohenstein EG, Chill ST and Sherrill CD, Assessment of the performance of the M05–2X and M06–2X exchange-correlation functionals for noncovalent interactions in biomolecules. *J Chem Theory Comput* **4**(12):1996–2000 (2008). https://doi.org/10.1021/ct800308k.
69. Zhao Y and Truhlar DG, The M06 suite of density functionals for Main group thermochemistry, thermochemical kinetics, noncovalent interactions, excited states, and transition elements: two new functionals and systematic testing of four M06-class functionals and 12 other functionals. *Theor Chem*

© 2025 The Author(s). *Biofuels, Bioproducts and Biorefining* published by Society of Industrial Chemistry and John Wiley & Sons Ltd.

19321031, 0, Downloaded from https://scijournals.onlinelibrary.wiley.com/doi/10.1002/bbb.2774 by Capes, Wiley Online Library on [28/08/2025]. See the Terms and Conditions (https://onlinelibrary.wiley.com/terms-and-conditions) on Wiley Online Library for rules of use; OA articles are governed by the applicable Creative Commons License

Account **120**(1–3):215–241 (2008). https://doi.org/10.1007/s00214-007-0310-x.
70. Pereira DH, Porta FAL, Santiago RT, Garcia DR and Ramalho TC, New perspectives on the role of frontier molecular orbitals in the study of chemical reactivity: a review. *Revista Virtual de Química* **8**(2):425–453 (2016). https://doi.org/10.5935/1984-6835.20160032.
71. Fukui K, The role of frontier orbitals in chemical reactions (Nobel lecture). *Angew Chem Int Ed Engl* **21**(11):801–809 (1982). https://doi.org/10.1002/anie.198208013.
72. Politzer P, Laurence PR and Jayasuriya K, Molecular electrostatic potentials: an effective tool for the elucidation of biochemical phenomena. *Environ Health Perspect* **61**:191–202 (1985). https://doi.org/10.1289/ehp.8561191.
73. Meng Y, Yang N, Qian Z and Zhang G, What makes an online review more helpful: an interpretation framework using XGBoost and SHAP values. *JTAER* **16**(3):466–490 (2020). https://doi.org/10.3390/jtaer16030029.
74. Li P and Zhang J-S, A new hybrid method for China's energy supply security forecasting based on ARIMA and XGBoost. *Energies* **11**(7):1687 (2018). https://doi.org/10.3390/en11071687.
75. Torlay L, Perrone-Bertolotti M, Thomas E and Baciu M, Machine learning–XGBoost analysis of language networks to classify patients with epilepsy. *Brain Inf* **4**(3):159–169 (2017). https://doi.org/10.1007/s40708-017-0065-7.
76. Sun B, Lam D, Yang D, Grantham K, Zhang T, Mutic S *et al*., A machine learning approach to the accurate prediction of monitor units for a compact proton machine. *Med Phys* **45**(5):2243–2251 (2018). https://doi.org/10.1002/mp.12842.
77. Bajusz D, Rácz A and Héberger K, Why is Tanimoto index an appropriate choice for fingerprint-based similarity calculations? *J Chem* **7**(1):20 (2015). https://doi.org/10.1186/s13321-015-0069-3.
78. Maulidiyah M, Nurdin M, Fatma F, Natsir M and Wibowo D, Characterization of methyl Ester compound of biodiesel from industrial liquid waste of crude palm oil processing. *Anal Chem Res* **12**:1–9 (2017). https://doi.org/10.1016/j.ancr.2017.01.002.
79. Hosseinzadeh-Bandbafha H, Kumar D, Singh B, Shahbeig H, Lam SS, Aghbashlo M *et al*., Biodiesel antioxidants and their impact on the behavior of diesel engines: a comprehensive review. *Fuel Process Technol* **232**:107264 (2022). https://doi.org/10.1016/j.fuproc.2022.107264.
80. Gupta D and Jain D, Chalcone derivatives as potential antifungal agents: synthesis, and antifungal activity. *J Adv Pharm Technol Res* **6**(3):114–117 (2015). https://doi.org/10.4103/2231-4040.161507.
81. Marquina S, Maldonado-Santiago M, Sánchez-Carranza JN, Antúnez-Mojica M, González-Maya L, Razo-Hernández RS *et al*., Design, synthesis and QSAR study of 2′-Hydroxy-4′-alkoxy chalcone derivatives that exert cytotoxic activity by the mitochondrial apoptotic pathway. *Bioorg Med Chem* **27**(1):43–54 (2019). https://doi.org/10.1016/j.bmc.2018.10.045.
82. Kobayashi T, Yanagita RC and Irie K, Synthesis and biological activities of simplified Aplysiatoxin analogs focused on the CH/π interaction. *Bioorg Med Chem Lett* **30**(24):127657 (2020). https://doi.org/10.1016/j.bmcl.2020.127657.
83. Wu J, Zhu S, Wu Y, Jiang T, Wang L, Jiang J *et al*., Multiple CH/π interactions maintain the binding of aflatoxin B1 in the active cavity of human cytochrome P450 1A2. *Toxins* **11**(3):158 (2019). https://doi.org/10.3390/toxins11030158.
84. Kiessling LL and Diehl RC, CH–π interactions in glycan recognition. *ACS Chem Biol* **16**(10):1884–1893 (2021). https://doi.org/10.1021/acschembio.1c00413.
85. Krone MW, Travis CR, Lee GY, Eckvahl HJ, Houk KN and Waters ML, More than π–π–π stacking: contribution of amide–π and CH–π interactions to Crotonyllysine binding by the AF9 YEATS domain. *J Am Chem Soc* **142**(40):17048–17056 (2020). https://doi.org/10.1021/jacs.0c06568.
86. Shimohigashi Y, Nose T, Yamauchi Y and Maeda I, Design of serine protease inhibitors with conformation restricted by amino acid side-chain-side-chain CH/? Interaction. *Biopolymers* **51**(1):9–17 (1999). https://doi.org/10.1002/(SICI)1097-0282(1999)51:1<9::AID-BIP3>3.0.CO;2-5.
87. Houser J, Kozmon S, Mishra D, Hammerová Z, Wimmerová M and Koča J, The CH–π interaction in protein–carbohydrate binding: bioinformatics and in vitro quantification. *Chem Eur J* **26**(47):10769–10780 (2020). https://doi.org/10.1002/chem.202000593.
88. Lavanya P, Ramaiah S, Singh H, Bahadur R and Anbarasu A, Investigations on the role of CH…O interactions and its impact on stability and specificity of penicillin binding proteins. *Comput Biol Med* **65**:85–92 (2015). https://doi.org/10.1016/j.compbiomed.2015.07.028.
89. Oku K, Watanabe H, Kubota M, Fukuda S, Kurimoto M, Tsujisaka Y *et al*., NMR and quantum chemical study on the OH···π and CH···O interactions between Trehalose and unsaturated fatty acids: implication for the mechanism of antioxidant function of Trehalose. *J Am Chem Soc* **125**(42):12739–12748 (2003). https://doi.org/10.1021/ja034777e.
90. Spackman PR, Turner MJ, McKinnon JJ, Wolff SK, Grimwood DJ, Jayatilaka D *et al*., CrystalExplorer: a program for Hirshfeld surface analysis, visualization and quantitative analysis of molecular crystals. *J Appl Crystallogr* **54**(3):1006–1011 (2021). https://doi.org/10.1107/S1600576721002910.
91. Saurabh S, Sivakumar PM, Perumal V, Khosravi A, Sugumaran A and Prabhawathi V, Molecular dynamics simulations in drug discovery and drug delivery, in *Integrative Nanomedicine for New Therapies*, ed. by Krishnan A and Chuturgoon A. Springer International Publishing, Cham, pp. 275–301 (2020). https://doi.org/10.1007/978-3-030-36260-7_10.
92. Barone V, Improta R and Rega N, Quantum mechanical computations and spectroscopy: from small rigid molecules in the gas phase to large flexible molecules in solution. *Acc Chem Res* **41**(5):605–616 (2008). https://doi.org/10.1021/ar7002144.
93. Zhang G and Musgrave CB, Comparison of DFT methods for molecular orbital eigenvalue calculations. *J Phys Chem A* **111**(8):1554–1561 (2007). https://doi.org/10.1021/jp061633o.
94. Vieira DF, Borges ID, Aguiar ASN, Duarte VS, D'Oliveira GDC, Vaz WF *et al*., A comparative structural analysis of arylsulfonamide chalcones with potential as a biofuel additive. *J Mol Struct* **1276**:134736 (2023). https://doi.org/10.1016/j.molstruc.2022.134736.
95. De Paula RLG, Carvalho FB, D'Oliveira GDC, Duarte VS, Santin LG, Pérez CN *et al*., Synthesis, crystal structure and molecular modeling of a novel chalcone-quinolone hybrid. *J Mol Struct* **1217**:128355 (2020). https://doi.org/10.1016/j.molstruc.2020.128355.
96. Morgan HL, The generation of a unique machine description for chemical structures-a technique developed at chemical abstracts service. *J Chem Doc* **5**(2):107–113 (1965). https://doi.org/10.1021/c160017a018.

© 2025 The Author(s). *Biofuels, Bioproducts and Biorefining* published by Society of Industrial Chemistry and John Wiley & Sons Ltd.

19321031, 0, Downloaded from https://scijournals.onlinelibrary.wiley.com/doi/10.1002/bbb.2774 by Capes, Wiley Online Library on [28/08/2025]. See the Terms and Conditions (https://onlinelibrary.wiley.com/terms-and-conditions) on Wiley Online Library for rules of use; OA articles are governed by the applicable Creative Commons License

97. Landrum G, Tosco P, Kelley B, Rodriguez R, Cosgrove D, Vianello R *et al*., Rdkit/Rdkit: 2024_09_1 (Q3 2024) Release (2024). https://doi.org/10.5281/ZENODO.591637.
98. Flitsch S, Neu PM, Schober S, Kienzl N, Ullmann J and Mittelbach M, Quantitation of aging products formed in biodiesel during the Rancimat accelerated oxidation test. *Energy Fuel* **28**(9):5849–5856 (2014). https://doi.org/10.1021/ef501118r.
99. D02 Committee, Test Method for Heat of Combustion of Liquid Hydrocarbon Fuels by Bomb Calorimeter (Precision Method) https://doi.org/10.1520/D4809-18.
100. Luque R, Lovett JC, Datta B, Clancy J, Campelo JM and Romero AA, Biodiesel as feasible petrol fuel replacement: a multidisciplinary overview. *Energy Environ Sci* **3**(11):1706 (2010). https://doi.org/10.1039/c0ee00085j.
101. Schober S and Mittelbach M, The impact of antioxidants on biodiesel oxidation stability. *Eur J Lipid Sci Technol* **106**(6):382–389 (2004). https://doi.org/10.1002/ejlt.200400954.
102. Burov EA, Ivanova LV, Koshelev VN and Adam TA, Additives to biodiesel fuels. *Chem Technol Fuels Oils* **59**(5):998–1002 (2023). https://doi.org/10.1007/s10553-023-01611-8.

Vitor S. Duarte

Vitor S. Duarte has a PhD in Environmental Sciences from the State University of Goiás. He is a postdoctoral research fellow at the State University of Goiás, focusing on small-molecule crystals and has participated in various innovation projects linked to the industrial production sector, focusing on structural analysis of pharmaceutical polymorphism, the development of bioactive compounds, supramolecular analysis and crystal engineering. He is experienced in theoretical calculations based on density functional theory and molecular topology using the quantum theory of atoms in molecules. He works on projects emphasizing innovation and the development of new products, with a particular focus on novel additives for biofuels.

Renata Layse G. de Paula

Renata Layse G. de Paula graduated in physics from the State University of Goiás, and has a Master's degree in physics from the Federal University of Goiás, with a focus on crystallography. Currently Renata Layse is a PhD candidate in the Natural Resources of the Cerrado program, conducting research on structural characterization and its technological applications, with experienced in operating single-crystal X-ray diffractometers and performing structural analysis of small molecules.

Leonardo R. Almeida

Leonardo R. Almeida is a postdoctoral research fellow at the State University of Goiás, focusing on small-molecule crystals, data science and machine learning applications for studying organic additives in biodiesel. He earned his PhD in Biomolecular Physics from the São Carlos Institute of Physics, University of São Paulo, where he investigated the structural, biochemical and biophysical properties of carbohydrate-active enzymes (CAZymes). He holds an MSc in Molecular Sciences (Physical Chemistry) from the State University of Goiás, where he specialized in single-crystal X-ray crystallography, supramolecular chemistry and density functional theory calculations to explore molecular electronic structures. His research experience includes organic synthesis of chalcones and azines, supramolecular chemistry, Hirshfeld surface analysis, computational chemistry, structural biology, enzyme kinetics and biophysics.

Giulio D. C. D'Oliveira

Giulio D. C. D'Oliveira has a PhD in Chemistry from the Federal University of Goiás. He researches the synthesis of new bioactive organic compounds. He currently serves as a Senior Analytical Development Analyst at Brainfarma Ind. Química e Farmacêutica S.A., focusing primarily on the development of analytical methods for quality control of raw materials.

Caridad N. Pérez

Caridad N. Pérez has a PhD in Chemical Engineering from COPPE at the Federal University of Rio de Janeiro and is currently a professor in the Graduate Programs in Chemical Engineering and Chemistry and a faculty member of the Chemical Engineering program at the Federal University of Goiás. She has experience in kinetics and heterogeneous catalysis. Her research focuses on basic solid catalysts for aldol condensation reactions of aldehydes and ketones. Her primary research area is the synthesis, characterization and antitumor evaluation of chalcones and their derivatives. Within this research line, she works on Michael addition reactions between glutathione and chalcones and their derivatives.

© 2025 The Author(s). *Biofuels, Bioproducts and Biorefining* published by Society of Industrial Chemistry and John Wiley & Sons Ltd.

19321031, 0, Downloaded from https://scijournals.onlinelibrary.wiley.com/doi/10.1002/bbb.2774 by Capes, Wiley Online Library on [28/08/2025]. See the Terms and Conditions (https://onlinelibrary.wiley.com/terms-and-conditions) on Wiley Online Library for rules of use; OA articles are governed by the applicable Creative Commons License

Jean M. F. Custódio

Jean M. F. Custódio is a biochemical scientist with hands-on experience in designing and developing independent and collaborative research projects focused on an in-depth understanding of T cell biology and the molecular mechanisms involved in immune system cell receptors for biomedical applications. Additionally, highly interested in biotechnology and skilled in the chemical processes underlying protein–small molecule interactions, such as drugs and synthetic compounds.

Valter H. Carvalho-Silva

Valter H. Carvalho-Silva has a PhD in Chemistry from UnB. Postdoctoral fellowship at the University of Perugia. Professor at UEG, coordinating MphysChem Lab and the High-Performance Computing Center. Research focuses on chemical kinetics, molecular modeling, AI in physicochemical transformations and environmental contaminant mitigation. He is a coordinator of the master's in molecular sciences at UEG, a founder of MinPro, a research consulting startup and a CNPq research fellow with publications in high-impact journals.

Andrea Lombardi

Andrea Lombardi is an Assistant Professor in Theoretical and Computational Chemistry at the University of Perugia. PhD in Theoretical and Computational Chemistry, with a focus on the application of advanced computational methods to understand molecular interactions and reaction mechanisms. His research interests include the development of new theoretical models and computational techniques to investigate complex systems, particularly in the fields of chemical reactivity, materials science and molecular dynamics.

Hamilton B. Napolitano

Hamilton B. Napolitano has a PhD in Biomolecular Physics from the University of São Paulo. He completed a postdoctoral fellowship at the State University of New York at Buffalo, USA. He served two consecutive terms (2009–2015) as a Member of the Higher Council of the Goiás State Research Support Foundation. He was a member of the Mathematical and Theoretical Crystallography commission of the International Union of Crystallography (2017–2023). He currently coordinates the Academic Master's and Doctoral Program for Innovation – MAI/DAI (2022–2027) and has led the Theoretical and Structural Chemistry Research Group in Anápolis since 2004. His expertise lies in Biomolecular Physics with an emphasis on Sustainable Development, and he is involved in several technological development projects in partnership with the industrial sector.

19321031, 0, Downloaded from https://scijournals.onlinelibrary.wiley.com/doi/10.1002/bbb.2774 by Capes, Wiley Online Library on [28/08/2025]. See the Terms and Conditions (https://onlinelibrary.wiley.com/terms-and-conditions) on Wiley Online Library for rules of use; OA articles are governed by the applicable Creative Commons License

© 2025 The Author(s). *Biofuels, Bioproducts and Biorefining* published by Society of Industrial Chemistry and John Wiley & Sons Ltd.